ANALYSIS OF THERMAL CONDUCTIVITY MODELS WITH AN EXTENSION TO COMPLEX CRYSTALLINE MATERIALS

A Dissertation
Presented to
The Academic Faculty

by

Abraham Greenstein

In Partial Fulfillment
of the Requirements for the Degree
Doctor of Philosophy in the
The George W. Woodruff School of Mechanical Engineering

Georgia Institute of Technology
August 2008

ANALYSIS OF THERMAL CONDUCTIVITY MODELS WITH AN EXTENSION TO COMPLEX CRYSTALLINE MATERIALS

Approved by:

Dr. Samuel Graham, Advisor
School of Mechanical Engineering
Georgia Institute of Technology

Dr. Sankar Nair, Co-Advisor
School of Chemical and Biomolecular Engineering
Georgia Institute of Technology

Dr. Martha Grover-Gallivan
School of Chemical and Biomolecular Engineering
Georgia Institute of Technology

Dr. David McDowell
School of Mechanical Engineering
Georgia Institute of Technology

Dr. Patrick Schelling
Department of Physics
University of Central Florida

Dr. Zhuomin Zhang
School of Mechanical Engineering
Georgia Institute of Technology

Date Approved: June 20 2008

ACKNOWLEDGEMENTS

First, I would like to thank my research advisor and mentor, Dr. Samuel Graham, for his guidance, support, and commitment to my growth as a researcher. I would also like to thank my co-advisor, Dr. Sankar Nair, for his support and contributions to this work and my education. Additionally, I would like to extend my appreciation to Yeny Hudiono for her collaboration on the zeolite work. I am also grateful to Dr. Patrick Schelling and Dr. Sylvie Aubry for mentoring me as an intern and continuing to collaborate with me on the gallium nitride work. Further, I would like to extend gratitude to committee members Dr. David McDowell, Dr. Zhuomin Zhang, and Dr. Martha Grover-Gallivan for their time and feedback. Finally, I am grateful to all of my friends and family members for their encouragement and support over the years.

TABLE OF CONTENTS

LIST OF TABLES

LIST OF FIGURES

SUMMARY

The calculation of the thermal conductivity of condensed matter has posed a significant challenge to engineers and scientists for almost a century. Thermal conductivity models have been successfully applied to many materials however many challenges still remain. One serious challenge is the inability of current thermal conductivity models to calculate the thermal conductivity of highly complex materials. Another challenge is managing error introduced by using an effective interatomic potential, for many materials this problem is exacerbated because their effective potentials have not been extensively used or characterized. Recent interest in nanostructures has initiated a new set of challenges and unanswered questions. This work addresses different aspects of the aforementioned challenges by using zeolite MFI and gallium nitride as case studies.

The first part develops a phonon based modeling methodology that can be used to study the thermal conductivities of complex nanoporous materials. In the second part interatomic potentials used to model gallium nitride are extensively tested, which includes an assessment of how well the potentials represent crystal anharmonicity. The third component of this work analyzes how phonon properties and bond anharmonicity differ in gallium nitride nanowires of different shapes and sizes.

Modeling the Thermal Conductivity of Zeolites

One major shortcoming of current models is their inability to calculate the thermal conductivity of highly complex materials. Calculations in the phonon picture of thermal transport frequently rely on simplified dispersion models, which neglect optical phonons.

Optical phonons frequently make substantial contributions to the thermal conductivity of complex materials, so current phonon based conductivity models are inapplicable. Molecular simulation has also been successful in calculating the thermal conductivities of many materials. However molecular simulation is purely classical and the thermal conductivities of complex materials often exhibit strong quantum effects, even at high temperatures. Zeolite MFI is used as a case study to develop a modeling methodology that can be used to calculate the thermal conductivity of highly complex materials. It is chosen as a case study because it is technically relevant and it is well characterized. Further many zeolites have the same crystalline structure but different compositions and some have the same composition but different crystalline structures. Thus zeolite materials can be used as a unique case study to understand structure-thermal property relationships in highly complex materials. The thermal conductivity of thick zeolite MFI films with different amounts of point defects, which have been grown by secondary hydrothermal synthesis, is measured with the 3-omega method. The new data is used to develop a new thermal conductivity modeling methodology for highly complex materials. The new methodology successfully reproduces the experimental data and provides physical insight into the conduction of heat in highly complex dielectric materials.

Evaluating the Quality of Interatomic Potentials Used to Model the Thermal Conductivity of Gallium Nitride

Experimental measurements of bulk gallium nitride thermal conductivity vary significantly amongst different samples. The large experimental variance makes phonon based thermal conductivity models, which rely on constants fitted to experimental data, unreliable. Therefore, molecular simulation is needed to calculate the thermal

conductivity of gallium nitride. Interatomic potentials used to simulate gallium nitride have not been as extensively used and tested as those that are used to model silicates and many other materials. Thermal conductivity is explicitly dependant upon the 3rd order derivatives of the interatomic potential with respect to atomic position. Effective interatomic potentials are approximations of the forces between atoms; every time the derivative of an approximation is taken the error gets magnified. As a result, it is expected that thermal conductivity is particular sensitive to the quality of the interatomic potential being used. The quality of two different potentials used to model gallium nitride are tested by calculating different harmonic phonon properties and thermal expansion coefficients then comparing the results with experimental data and each other. It is found that an effective potential that yields accurate results for harmonic material properties may be unable to correctly calculate properties, like thermal expansion, that are highly dependant upon crystal anharmonicity.

Lattice Dynamics of Gallium Nitride Nanowires

Gallium nitride nanowires are increasingly being used in the development of next generation solid state devices. Device performance is substantially affected by the temperature distribution and the formation of hot spots in the device, both of which are dependant upon the thermal properties of the device. Many confinement effect issues are still not well understood. Calculations of the phonon spectrum, specific heat, average phonon speed, and homogenous Gruneisen parameter are performed on gallium nitride nanowires of different shapes and sizes. It is found that harmonic phonon properties of nanowires differ substantially from the bulk but are only weakly dependant on wire size and moderately dependant on wire shape.

CHAPTER 1

INTRODUCTION

Thermophysical properties of materials are often key parameters in the determination of the thermal response, performance, and reliability of many engineering devices. As such, it is highly desirable to control or tailor the thermal properties of materials for specific applications. In contrast to the technological revolution in modifying the electrical transport properties, understanding and methods to manipulate the thermal conductivity of solid state materials is very limited. The theoretical basis of structure-thermal property relationships in solid state materials has be described through the Boltzmann transport equation for the past 80 years. However, the current application of the theory relies on many simplifying assumptions in order to obtain tractable descriptions of thermal transport. The objective of this work is to improve upon current thermal conductivity modeling paradigms. This will yield a more accurate understanding of phonon physics and allow an extension of current models to complex and exotic materials. The proposed work studies the thermal properties of a diverse set of complex materials (zeolites and nanostructured GaN). Zeolites and GaN provide interesting case studies because they are both technically relevant and occur in complex forms, which require advances in the state of the art in thermal transport modeling. The wide variety of materials and techniques provide a thorough and diverse framework for modeling and understanding thermal conduction in complex materials which can be extended to other complex oxides and semiconductors which are currently underdevelopment today.

1.1 Zeolites

Zeolites are nanoporous mixed-oxide crystals with complex structures formed by corner-sharing oxide tetrahedral (TO4; T=Si, Al, etc.). There are more than 100 zeolite structures known, as well as a large number of other frameworks obtained by combination with elements favoring octahedral and pentahedral coordination. The capability of altering the composition of a given zeolite (e.g., by lattice atom substitution or by introducing metal cations and organic molecules into the pores) while maintaining the same crystal structure, or conversely the ability to synthesize different crystal structures with the same composition, makes them extraordinarily versatile materials with interesting structure-function relationship[1] as well as many important applications[2]. Newly emerging applications of zeolites include low-k dielectric films for computer chips, materials for adsorption cooling devices[3,4], and hosts for nanotube/wire arrays[5]. More generally, complex oxides which include zeolites are being developed as transparent semiconductor and power generation materials, transparent electrodes for displays and flexible electronics and dielectric films. Theoretical interest in the thermal transport properties of zeolite materials originates primarily from their suitability as a model system containing complex, yet well-defined and characterizable, nanostructural features (such as an ordered nanopore network, lattice substitution sites, metal cations or organic species adsorbed in the pores) that interact with heat carrying phonons, thus offering a number of opportunities for developing and testing models for thermal conductivity in complex crystals. The rich structural complexity of these materials, as well as the increasing significance of thermal transport properties inherent in their emerging applications, justify detailed study of their thermal transport properties, of

which current knowledge is relatively limited. There are both experimental difficulties as well as theoretical challenges in describing thermal transport in complex materials with large unit cells[6-9]. The thermal conductivity of zeolites is usually measured by compacting zeolite powders into disks[9,10]. Measurements on powder samples are particular error prone because the presence of microscopic voids in the compacted disks skew the measured value of thermal conductivity and methods to correct the data are approximate[9]. Computational approaches have relied on classical molecular dynamics simulations[7,8,11], which provide qualitative insight, but do not easily allow discrimination of the contributions from several possible phonon scattering mechanisms nor describe well the quantum statistical aspects of the phonon physics. Deviations from classical behavior of thermal properties are particularly large for zeolites. This is because zeolites have many high frequency phonons, which make substantial contributions to thermal conductivity and high frequency phonons only behave classically at high temperatures. This is evidenced in large discrepancies[7,8] between measured and computed thermal conductivities.

The zeolite study presented here combines systematic variation of zeolite composition, measurements of thermal conductivity using polycrystalline zeolite films which are more reliable than measurements on compacted powders, and modeling of thermal transport incorporating detailed input from lattice dynamics calculations (made with a high-quality interatomic potential). This approach allows separation and analysis of the structural and dynamical factors that influence the conductivity. The important zeolite MFI has been chosen as a well-characterized model system.

1.2 Zeolite Modeling Challenges

Modeling the thermal properties of zeolites is particularly problematic because no current techniques used to model thermal transport can estimate their thermal conductivities. Furthermore, current techniques are even incapable of giving the correct qualitative behavior of how zeolite conductivity changes with temperature[6,12]. The two approaches used to model thermal properties are molecular dynamics and lattice dynamics. Molecular dynamics cannot be used to calculate the thermal conductivity of zeolites because it is classical. Classically the thermal conductivity of a material can only decrease with rises in temperature. This is because the classical specific heat of a material is constant, but real materials behave quantum mechanically so their specific heats increase with temperature and become constant in the classical limit. Even at temperatures well above room temperature, Zeolite conductivities frequently increase with rising temperature. Hence, molecular dynamics is incapable of providing realistic description of zeolite conductivity.

In lattice dynamics, the material being modeled is treated as a gas of interacting phonons. Phonons are quantized lattice vibrations, which are analogous to photons. The modern theory of thermal conduction by phonons was primarily developed by Peierls in the late 20's[13]. In the phonon picture of thermal transport the non-equilibrium phonon distribution, which causes a net heat flux, is governed by the Boltzmann transport equation. However the scattering term in the equation is exceedingly complex precludes any kind of analytical solution and can only directly be solved by numeric iteration. In the early 50's Klemens[14] introduced the relaxation time approximation to the Boltzmann equation. In the relaxation time approximation the Boltzmann transport equation is

linearized and it is assumed that the non-equilibrium phonon distributions scatter back to equilibrium at an exponential rate. The time constant in the exponential is called the relaxation time. Klemens used his relaxation time approximation to derive an approximate expression for thermal conductivity. He then developed semi-analytical relaxation time expressions that relied on fitted parameters to make some conductivity calculations[14,15]. To make his computations tractable, Klemens used many of the same assumptions used in the Debye specific heat model. The Debye specific heat model assumes there are only three polarizations that have the same isotropic dispersion, which go linearly from zero to some cutoff frequency. With the help of the Debye model and the use of fitted constants he was able to calculate the thermal conductivity. While there have been some modifications and improvements made to the Klemens model[16-18], most conductivity models that use the relaxation time approximation still rely on a highly simplified dispersions[9,17-22]. Hence, they are inapplicable to highly complex materials.

1.3 Gallium Nitride

Gallium Nitride is a wide band gap semiconductor with large carrier mobilities and electrical breakdown field and is considered an excellent material for use in high power semiconductor devices[23]. At present, gallium nitride is being developed for rf and microwave communications applications with broad military and commercial appeal. Due to the tunability of its bandgap through the formation of AlGaN and InGaN compounds, gallium nitride has also become the workhorse material for the solid state lighting market, enabling the development of high powered and efficient LED sources. The aforementioned devices utilize gallium nitride in thin film form (20 – 2000 nm) with primarily a hexagonal wurtzite structure, although it may be found in a cubic zinc blend

structure as well. These crystal structures are almost always grown heteroepitaxially on substrates which are not well lattice matched, thus introducing a number of defects in the crystals which may impede thermal performance.

In contrast to the thin films, gallium nitride nanowires are now being used to make new and unusual optoelectronic devices and circuit components. Gallium nitride nanowires have been used to make blue laser[24]. They have also been coated with different materials to create high efficiency multicolor diodes[25]. Next generation optical nanodevices are also being made with gallium nitride nanowires. Huang et al[26] used high quality gallium nitride nanowires to created field effect transistors with large carrier mobilities. The observed carrier mobilities show that gallium nitride nanowires are particularly well suited for use in next generation functional electronics. Both bulk and nanostructures gallium nitride have a number of optoelectronic applications and are expected to play a prominent role in next generation microelectronics. Despite its technological relevance the thermal properties of nanostructured gallium nitride are not well understood.

1.4 Gallium Nitride Modeling Challenges

There have been a few studies which have theoretically analyzed the conductivity of gallium nitride[27,28]. However, these studies used many unphysical assumptions, such as linear dispersion and neglect of the optical phonons, which may be valid for bulk gallium nitride but confinement effects cause nanostructures to have complicated dispersions which cannot validly be modeled without taking into account the optical phonons. These calculations have also relied on parameters fitted to experimental data, but there is a large range of measured values of the bulk thermal conductivity of gallium

nitride. This large variation in values is caused by a lack of structurally consistent samples and makes it difficult to interpret the physical meaning of the fitted parameters.

The lack of consistent thermal conductivity data for bulk and nanowire gallium nitride necessitates the use of theoretical tools such as lattice dynamics and molecular simulation to estimate conductivity. The accuracy of both these techniques is limited by the quality of the interatomic potential used. Effective potentials for gallium nitride have not been as extensively tested as those for other materials and thermal conductivity is particularly sensitive the quality of the interatomic potential. The gallium nitride study presented here asses the quality of two commonly used effective potentials[29,30] by calculating the density of states, specific heat, and thermal expansion of bulk gallium nitride and comparing them with experimental data. Then the effects of nanowire size and shape on phonon spectrum, specific heat, phonon speed, and homogenous Gruneisen parameter are studied. This analysis helps explain why nanowire conductivity is different from bulk, provides a framework for understanding thermal properties in nanostructures, and assesses the quality of interatomic potentials to help guide future theoretical investigations.

1.4 Dissertation Objectives

The work presented in the dissertation has three main objectives:

- **Measure and model the thermal conductivities of zeolites**. The measured thermal conductivities presented in this work make a valuable contribution to the field because they are the first measurements performed on films, so they are far more reliable than existing measurements on powders. The set of systematic and consistent data provides invaluable information that is used to develop a new

thermal conductivity modeling methodology that is applicable to highly complex materials. The new methodology is used to model seven different zeolites and explains why zeolites have low thermal conductivities, why small amounts of impurities drastically lowers the thermal conductivity, and how cations in the pores affect the thermal conductivity.

- **Assess the quality of interatomic potentials used to model gallium nitride.** The calculated thermal conductivity is far more sensitive to the interatomic potential than other material properties. Lattice dynamical calculations are done on bulk gallium nitride with a Stillinger Weber[29] and a Tersoff[30] potential. It is shown that the two potentials exhibit drastically different crystal anharmonicity and are expected to predict different thermal conductivity values.
- **Analyze the effects of nanowire shape and size on the phonon spectrum**. Lattice dynamical calculations are performed on three different nanowires of varying shape and size. For each nanowire density of states, specific heat, average phonon speed, and homogenous Gruneisen parameters are calculated. It is found that all properties are substantially different from that of bulk gallium nitride, but the harmonic properties are only weakly dependant on nanowire size.

CHAPTER 2

BACKGROUND THEORY

This chapter starts with an overview of traditional phonon relaxation time models. After that the theories of phonons and phonon thermal properties are treated in more detailed fashion. Then the chapter concludes with a brief exposition on interatomic potentials.

There are two ways to model conductive heat transfer through a crystalline solid. Heat can be thought of as energy transfer due to atoms in real space, the other is to think of heat as being carried by superimposed quantum lattice waves, also known as phonons, which exist in wave space. A dielectric crystalline solid can be thought of as a phonon gas, heat excites phonons and the phonons drift through the solid carrying the heat.

In the phonon picture, a solid is modeled as a spring-mass network where the atoms behave as point masses and the chemical bonds as springs. Phonons are linear combinations of the normal modes of vibration of the spring-mass network. By superimposing the normal vibrations packets of energy localized in real and wave space can be constructed; these localized energy packets are the phonons. A schematic of a lattice wave in simple solid is shown in Figure 2.1. The spring-mass network is perfectly harmonic and real crystals are anharmonic. A harmonic crystal has an infinite conductivity. If one were to shake a mass in a harmonic spring-mass network the signal would propagate across the network undamped and uninhibited. Therefore the perfectly harmonic crystal fails to provide an adequate model for conductivity. If the crystal is

weakly anharmonic, harmonic eigenstates with eigenvalues corrected for anharmonicity can be used to adequately model the conductivity[22,31]. The harmonic eigenvalues are always real, while the anharmonic eigenvalue corrections are complex and the imaginary part is the inverse of phonon lifetime.

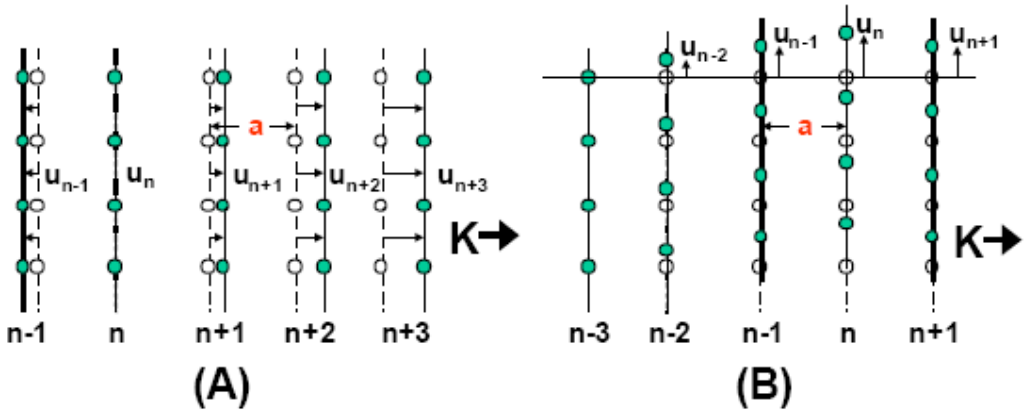

Figure 2.1 Schematic of transverse and longitudinal lattice waves. The picture is taken from Huxtable[32]. A shows a snap shot of a longitudinal vibration where the atoms displace (white dots are equilibrium positions and green are current positions) in the same direction as the wave vector. B shows a transverse vibration where the atoms displace in the direction perpendicular to the wave vector. The picture is conceptually illuminating but should not be interpreted literally because lattice ways are typically much more complex and do not always have readily defined longitudinal and transverse vibrations.

The quantum theory of light provides a good metaphor for understanding phonons, normal modes of vibration, and energy eigenstates of the phonon gas. In the theory of light the quantum mechanical Fock states are analogous with the energy eigenstates of the phonon gas. The classical eigenstates of Maxwell's electromagnetic wave equation correspond to the normal modes of vibration and photons are analogous with phonons. There are many mathematical similarities between the electromagnetic field and the harmonic crystal. Both have a one to one correspondence between energy eigenstates and normal modes and the phonon/photon occupancies of the eigenstates determine the amplitude of the normal vibrations.

The heat capacity of a real gas is the sum of the heat capacities of its molecules. Like a real gas the solid or 'phonon gas' specific heat is simply a sum of the specific heat of the individual phonons, furthermore the expression for conductivity of the 'phonon gas' is analogous with that of a real gas and is[14]:

$$k_j = \sum_{\mathbf{K}p} c_p(\mathbf{K})\left(\mathbf{v}_p(\mathbf{K})\cdot\hat{\mathbf{j}}\right)^2 \tau_p(\mathbf{K}) \tag{2.1}$$

The subscript on the conductivity labels the direction of interest. The summation goes over all unique physically meaningful phonon wave vectors K and dispersion branches p, so it is a sum over all phonon states (a phonon state is a also called a mode). The number of dispersion branches is equal to three times the number atoms in a unit cell, the set of all unique physically meaningful phonon wave vectors are all contained in a volume in wave space called the Brillouin zone, $c_p(\mathbf{K})$ is the specific heat of all the phonons in a mode, $\mathbf{v}_p(\mathbf{K})$ is the velocity of a phonon in a given mode and it is projected onto the direction of interest, and $\tau_p(\mathbf{K})$ is the relaxation time, which is the time it takes an over excited phonon state to return to equilibrium.

2.1 The Debye Model

Dispersion relationships can be complex and not always easy to calculate; calculating them requires a detailed knowledge of the interatomic potentials and the equilibrium atomic coordinates at T=0. For some materials like silicon the dispersion can be readily and quickly calculated but for highly complex materials calculation of the dispersion requires careful energy minimization of the crystal lattice and long computation times. An example of dispersion in a simple material can be seen in Figure 2.2. There are six branches but because of degeneracy only four can be seen on the

graphs notice that at long wave lengths (small wave vectors) the acoustic branches become linear.

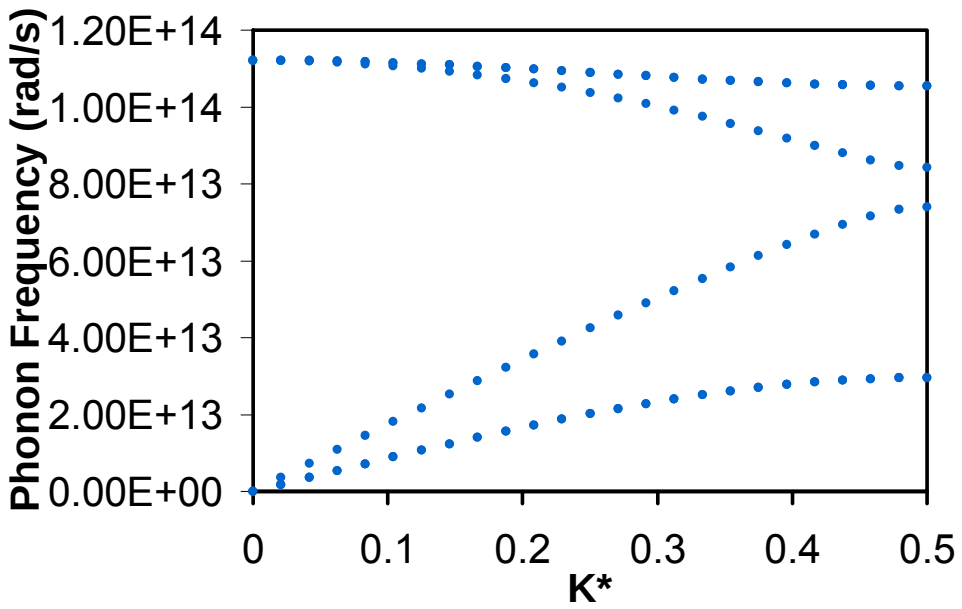

Figure 2.2 Calculated phonon dispersion for silicon along the (1 0 0) direction of the Brillouin zone. The x-axis is the non-dimensional position along the (1 0 0) edge of the Brillouin zone. The non-dimensional coordinates shown start at the center of the zone and go to the zone edge.

The vast majority of thermal property calculations in the phonon picture do not utilize the actual dispersion instead they use a simplified dispersion originally developed by Debye. In 1912 Debye proposed a simple model of dispersion to enable calculation of specific heat[33]. The model is known as the Debye model. In the Debye model there are only three dispersion branches and they are linear, isotropic, and degenerate. There are three different branches because in a continuum there are two different transverse ways the medium can vibrate and one longitudinal. The linear dispersion has a slope set

equal to the speed of sound, because long wave length acoustic phonons are responsible for the propagation of sound in a solid and it is known that sound has a linear dispersion. The isotropic and degenerate approximations are merely simplifications. In essence the Debye model treats the dispersion as that of sound in an isotropic continuous medium; as a result the Debye dispersion is a good approximation for wave lengths much greater than the interatomic spacing of the lattice.

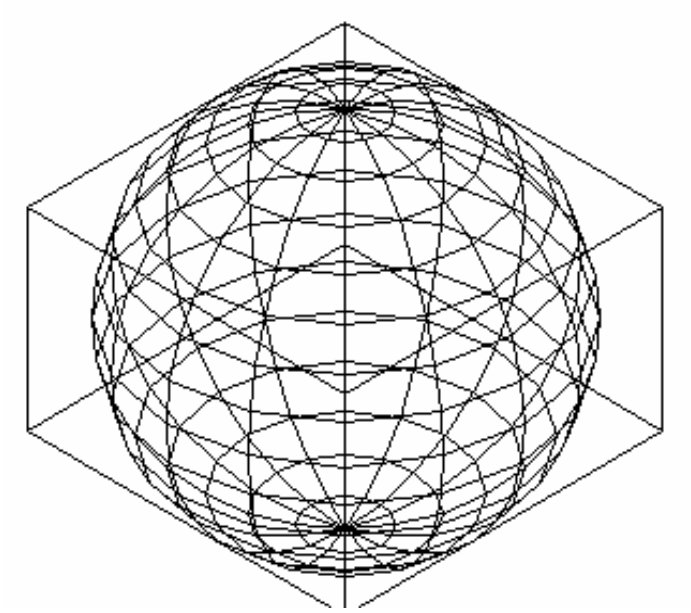

Figure 2.3 Comparison of the actual Brillouin zone of an orthorhombic crystal and the Brillouin zone of the Debye model.

Waves in a continuous medium do not have a maximum wave-vector, but waves in a crystal lattice do. A lattice is discrete not continuous as a result the maximum wave vector is dependant on the lattice constants of the solid. For a one dimensional lattice with a lattice constant of a, the shortest possible wave length is 2a, because wavelengths shorter than 2a are not physically meaningful. As a result, the one dimensional lattice has

a cut off wave vector of π/a. For an actual three dimensional crystal the cutoff is a closed surface (the enclosed volume is the Brillouin zone). In the Debye model the Brillouin zone is a sphere that has a radius equal to a magnitude called the cutoff wave-vector. Figure 2.3 shows a schematic comparing the Brillouin zone of a crystal with an orthorhombic unit cell, with the Brillouin zone predicted by the Debye model. The value of the cutoff wave vector is obtained from the average interatomic spacing in a crystal and results in a Debye Brillouin zone that has a volume equal to the number atoms in a unit cell times the volume of the actual Brillouin zone. Dispersion in the Debye model has following simple form[34],

$$\begin{aligned} &\omega(\mathbf{K}) = v_{sound}\,|\mathbf{K}| \\ &0 \le |\mathbf{K}| \le K_{cut} \\ &K_{cut} = \left(6\pi^2 \frac{N}{V}\right)^{1/3} \end{aligned} \tag{2.2}$$

Debye used his simplified model to calculate the heat capacity of dielectric materials, which is dependant only on phonon dispersion.

The heat capacity of all the phonons in a given mode is,

$$c_p(\mathbf{K}) = k_B \left(\frac{\hbar\omega_p(\mathbf{K})}{k_B T}\right)^2 \frac{\exp\left(\frac{\hbar\omega_p(\mathbf{K})}{k_B T}\right)}{\left(\exp\left(\frac{\hbar\omega_p(\mathbf{K})}{k_B T}\right)-1\right)^2} \tag{2.3}$$

The total heat capacity is the sum of the heat capacities of all the modes.

$$C_v = \sum_{\mathbf{K}p} c_p(\mathbf{K}) \cong \frac{V}{(2\pi)^3} \sum_p \int c_p(\mathbf{K}) dK^3 \tag{2.4}$$

In the third term of the above expression the summation over all wave-vectors is replaced with an integral, in most cases this results in negligible error. By using a change of

variable and exploiting the isotropy of the Debye dispersion, the specific heat in the Debye model can be written as,

$$C_v = 9Nk_B\left(\frac{T}{\theta_D}\right)^3 \int_0^{\theta_D/T} \frac{x^4 e^x}{\left(e^x - 1\right)^2} dx \tag{2.5}$$

θ_D is the Debye temperature and has the following definition

$$\theta_D \equiv \frac{\hbar}{k_B} v_s K_{cut} = \frac{\hbar}{k_B} v_s \left(6\pi^2 \frac{N}{V}\right)^{1/3} \tag{2.6}$$

The above expression is of great convenience because just by knowing the speed of sound in a solid the heat capacity can be predicted at all temperatures. While the Debye temperature can be calculated from the speed of sound it is often fitted to experimental data.

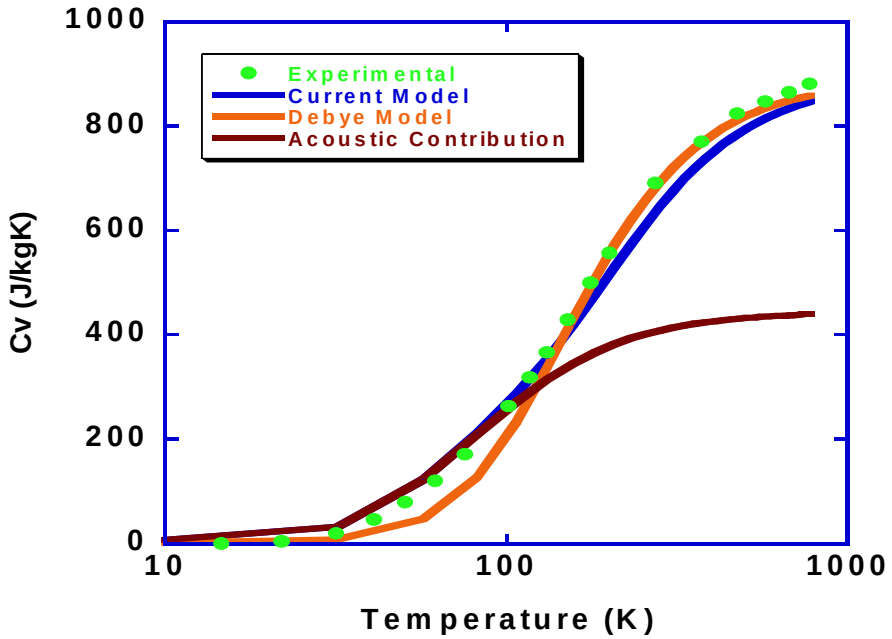

Figure 2.4 Specific heat of silicon. The figure is from Greenstein et al[6] 'current model' labels the specific heat calculated from the full dispersion

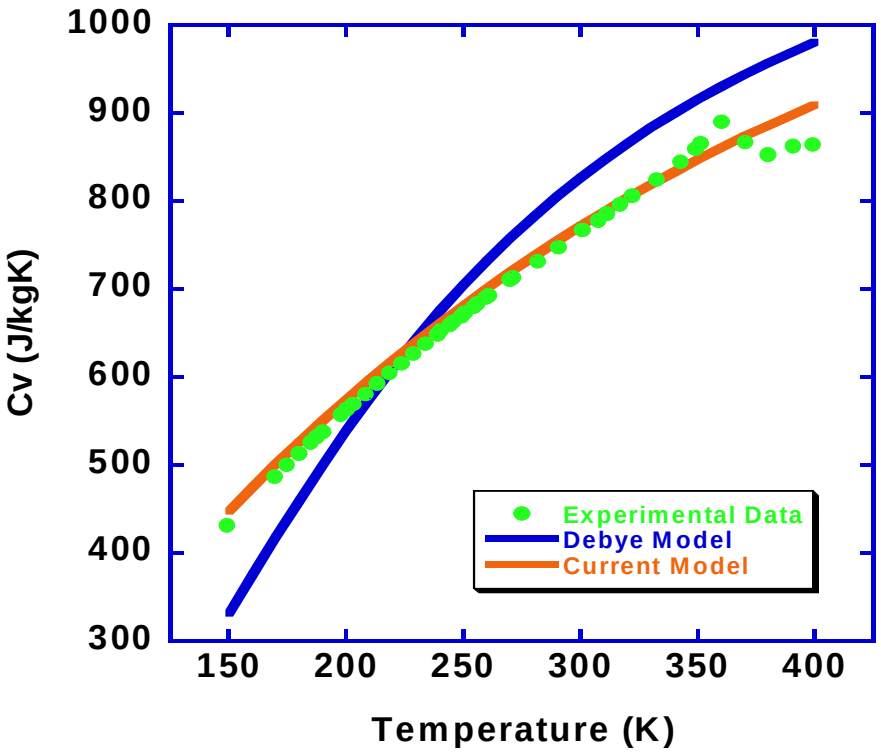

Figure 2.5 Specific heat of zeolite MFI the figure is from Greenstein et al[6] 'current model' labels the specific heat calculated from the full dispersion

The Debye model has done an excellent job of predicting the specific heat of many materials; this is not surprising because in actuality the Debye model is an interpolation formula. In the high temperature limit every phonon mode of a harmonic crystal has a constant heat capacity equal to Boltzmann's constant. As a result, the Debye model will give the correct high temperature specific heat because the cutoff wave-vector in the Debye model is defined so that the number of phonon states in the Debye model is equal to the actual number of phonon states. In the low temperature limit, only the long wave-length acoustic phonons contribute to the specific heat and for those phonons the Debye model is quite reasonable. For specific heat the Debye model almost always gives good results in the low and high temperature limits and the specific heat at intermediate temperatures is a clever interpolation of the specific heat at those limits. For simple materials like silicon the Debye model predicts the specific heat successfully at all temperatures. Figure 2.4 shows the specific heat of silicon calculated from the Debye model and directly from the full dispersion; the Debye model prediction is only slightly less accurate than the full dispersion calculation. However, for many complex crystals like zeolites the Debye model does a poor job of predicting the specific heat at many temperatures. The specific heat of zeolite MFI is shown in Figure 2.5 the Debye model is incapable of predicting the right trend but the specific heat calculation that uses the full dispersion is accurate.

2.2 Thermal Conductivity and the Debye Model

In 1951 Klemens[14] developed the relaxation time theory for phonons and made some of the first thermal conductivity calculations. By using the Debye model of dispersion he arrived at the following thermal conductivity expression,

$$k = 3Nk_B\left(\frac{T}{\theta_D}\right)^3 \int_0^{\theta_D/T} \frac{x^4 e^x}{\left(e^x - 1\right)^2} v_s^2 \tau(x) dx \tag{2.7}$$

To make the calculations tractable he used the Debye dispersion model and a semi-empirical relaxation time model that relied on fitted constants. His calculations agreed well with experiment but the use of fitted constants probably covered up some error caused by the Debye spectrum. Furthermore, the crystals he did calculations on have their conductivities dominated by long wave length phonons, which the Debye model does a decent job of approximating. However, the Debye model's treatment of the optical phonons is completely inadequate. Instead of explicitly treating them it has the acoustic branches occupying more wave space to compensate for the states not accounted for by explicitly including the optical branches. This results in treating the optical branches as if they were moving at the speed of sound, but in fact they are moving much slower. This is not serious problem for the crystals that Klemens studied because in those crystals the scattering of the optical branches was much stronger than that of the acoustic branches so they are unimportant to conduction anyway.

Since Klemens first introduced his model there have been several improvements on the use of the Debye dispersion in conductivity. Holland[17] made improvements by treating the transverse and longitudinal branches separately and by breaking the dispersion up into two separate linear regimes in the Brillouin zone. The Tiwari[18] model of dispersion, used a slightly more sophisticated functional form for the dispersion; where the wave vector is treated as a 2nd order polynomial with respect to frequency. However, all these models only treat the acoustic dispersion and neglect the optical dispersion. As

a result, a new modeling methodology is needed for highly complex crystals that have many optical branched that contribute substantially to the conductivity.

2.3 Modeling the Relaxation Time

The relaxation time is defined as the average time it takes a phonon mode, with more phonons than its equilibrium occupancy, to return to its equilibrium occupancy. There is no clear way to model the relaxation time. Time-dependant quantum perturbation theory provides a theoretical framework for calculating phonon lifetimes[15,35], but phonon lifetime is the average time a single phonon exists before it is scattered and not the time it takes a non-equilibrium occupancy of a phonon mode to decay to its equilibrium occupancy. Further, a direct calculation of the phonon lifetimes is extremely expensive and can only be done for the simplest of crystals[36-39] and the relaxation time is an even more complex quantity.

There are many different mechanisms that cause phonons to scatter into different states. Phonons can scatter off of different kinds of crystalline defects, such as point defects, dislocations, stacking faults, grain boundaries, and interfaces, and off each other. A rigorous treatment of all phonon scattering mechanisms for any but the simplest cases is too expensive to be done. As a result, there are different semi-empirical approximations, which rely on fitted constants that can be used to estimate phonon scattering from different scattering mechanisms. To calculate the net relaxation time from the different scattering mechanisms Matthiessen's rule is used[15,40]. Matthiessen's rule treats all scattering processes as occurring in parallel with each other and is,

$$\frac{1}{\tau_{total}(\mathbf{K})} = \sum_i \frac{1}{\tau_i(\mathbf{K})} \tag{2.8}$$

In the above expression i is a summation over all the different scattering processes. Models for the scattering rates from different structural defects are readily available in the literature[22,35,40-42]. There are also models for modeling the relaxation time for phonon-phonon scattering[14,16,43,44]. For defect scattering phonon lifetime and relaxation time are almost identical. For phonon-phonon scattering the relationship between lifetime and relaxation time is more complex.

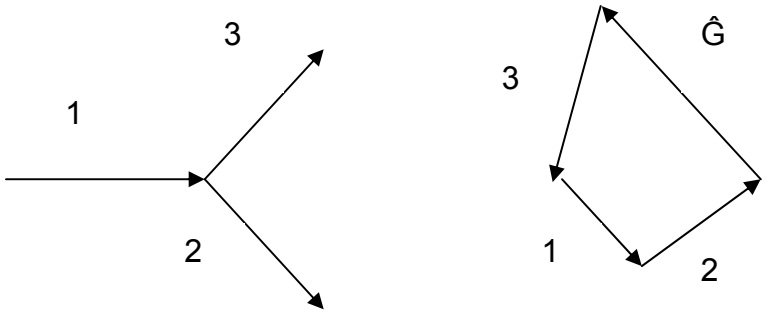

Figure 2.6 Umklapp and normal processes. The first diagram shows a normal process, were phonon 1 splits into phonons 3 and 3; wave vector is conserved and heat flows unimpeded. The second diagram shows an umklapp where phonons 1 and 2 collide to make phonon 3 but in the process the phonons undergo Bragg reflection and the resulting wave vector is in the opposite direction; wave vector is not conserved and heat flow is directly impeded. The first diagram shows a phonon splitting while the second shows two phonons merging but both normal and umklapp processes can occur when phonons merge or when a phonon splits.

Phonon scattering by defects is far simpler than phonon-phonon scattering because all defect scattering events directly contribute to the thermal resistance; this is not the case for phonon-phonon scattering. There are two different types of phonon-phonon scattering events umklapp scattering and normal scattering. A schematic of the

two processes is shown in Figure 2.6. Both types of events occur when either two phonons merge into one or when one phonon splits into two. A normal scattering event occurs when the net wave-vector before the collision is equal to the net wave vector after the collision. An umklapp event occurs when there is a scattering process and during the process the phonons undergoes Bragg reflection so the net wave-vector is flipped back. Normal processes do not directly contribute to thermal resistance they merely redistribute the phonons and the heat continues to drift unimpeded. By 'flipping' the net wave vector Umklapp processes cause a direct resistance to the flow of heat. The relationship between the two types of scattering and how they are related to relaxation time is a little ambiguous.

The simplest relaxation time model is the single mode relaxation time approximation or the SMRT approximation. It assumes that all phonon modes decay as if every other mode were in equilibrium and is equivalent to assuming that the relaxation time is the same as the lifetime. This approximation has been successfully used in the past[17,45] but it is unphysical because not all phonon scattering processes contribute to the thermal resistance. Another common approach developed by Callaway[16] is to separate phonon-phonon scattering processes into Umklapp and Normal processes. Then have one term where the two scattering processes are both treated as resistive and another term that corrects for phonon drift do to normal processes. Yet another approach is to set the phonon-phonon relaxation time equal to the time between Umklapp scattering events, so the Normal processes are completely neglected[20]. This is done because normal processes do not directly contribute to the thermal resistance. For many crystals normal scattering does not occur as frequently as umklapp scattering and is unimportant; for these crystals

all of the above approaches are equivalent. There are more even models[22,44], which are not discussed here, that relate frequency of normal and umklapp scattering events to phonon-phonon relaxation time. In phonon-phonon practice relaxation time is frequently calculated with semi-empirical formulas[14,16,21], which depend on parameters that are fitted to experimental data. This is done because with the exception of the simplest crystal systems calculation of phonon lifetime is too expensive to be practical.

2.4 Normal Coordinates and the Calculation of Phonon Dispersion

The earlier discussion on phonon dispersion was based largely on heuristic arguments. One of the goals of this work is to incorporate full phonon dispersion into conductivity models. This section outlines some of the theory needed to understand how to calculate phonon dispersion. An atomic lattice can be modeled as a set of coupled harmonic oscillators. When expressed in xyz coordinates the equations of motions of the masses in a mass spring network are highly complex and coupled with one another. However, when expressed in terms of different coordinates the equations of motion become much simpler. This is not a feature unique to coupled oscillators; many dynamical systems are much easier to analyze with coordinates other than Cartesian ones. For example, the dynamics of pendulum are simpler to analyze in polar coordinates than in Cartesian ones. The most convenient set of coordinates for analyzing coupled harmonic oscillators are called normal coordinates and like any other valid set of coordinates provide a complete description of the systems. The normal mode coordinates greater simplify the equations of motion because they decouple them from each other, so each normal mode coordinate is independent from all the other ones. As a result, a spring

mass system which is an n-body problem in Cartesian coordinates becomes n one-body problems in normal coordinates.

In the normal coordinate picture, the dynamics of point masses in a mass spring network are not expressed as individual mass displacements. Instead the system dynamics are expressed as linear combinations of coupled vibrations. The frequencies of the collective vibrations are called the normal mode frequencies. The magnitude of a normal coordinate, which is usually a complex number, is the amplitude of the collective vibration and any configuration of the system can be expressed in terms of normal coordinates.

Finding the normal modes of vibration of a mass spring network is a well documented problem that yields simple equation of motion[46]. Therefore it is desirable to approximate the atomic equations of motion in a crystalline lattice as set of point masses connected by springs. This can be done by expressing the potential energy of a crystal lattice in Taylor series, with respect to the atomic displacements, which is

$$\Phi = \Phi_o + \sum_{il\alpha} \frac{\partial \Phi}{\partial u_{il\alpha}} du_{il\alpha} + \frac{1}{2!} \sum_{il\alpha,\, jm\beta} \frac{\partial^2 \Phi}{\partial u_{il\alpha} \partial u_{jm\beta}} du_{il\alpha} du_{jm\beta} + \frac{1}{3!} \sum_{il\alpha,\, jm\beta, kn\gamma} \frac{\partial^3 \Phi}{\partial u_{il\alpha} \partial u_{jm\beta} \partial u_{kn\gamma}} du_{il\alpha} du_{jm\beta} du_{kn\gamma} + \ldots \tag{2.9}$$

In the preceding expansion atomic displacements, u are treated as the independent coordinates which the potential energy Φ is expanded about, ijk run over all atoms in the unit cell lmn run over all unit cells and $\alpha\beta\gamma$ over all directions, so $u_{il\alpha}$ is the displacement of the ith basis atom in the lth unit cell in the α direction. The zeroth order term is set to zero because only changes in the energy are important, the first order term is always zero for a crystal in mechanical equilibrium[47], so the dominant term is the second order term. As a result, many crystal properties and behaviors are adequately

modeled by neglecting the third and higher order terms. This is called the harmonic approximation. Many crystal properties, like specific heat and mean atomic displacement can be calculated with the harmonic approximation. However, there are many other crystal properties and phenomenon for which the harmonic approximation is completely invalid these include thermal expansion coefficient, thermal conductivity, and 2nd order phase transitions. Solving the full anharmonic equations of motion is not feasible however there are approximate techniques, whose appropriateness depends on what is being calculated, that can be used to estimate the anharmonicity.

Normal coordinates can be also be used as a set of independent coordinates for the Taylor expansion. The normal mode coordinates for a crystal are defined as[48]

$$Q_p(\mathbf{K},t) = \frac{1}{N^{1/2}} \sum_{il\alpha} m_i^{1/2} \exp\left(-i\mathbf{K}\cdot\mathbf{r}_{il}\right) e^*_{pi\alpha}(\mathbf{K}) u_{il\alpha}(t) \tag{2.10}$$

N is the number of unit cells in the crystal, m is the atomic mass, the summation is over all atoms in a unit cell, all unit cells in the crystal, and all directions. r is the equilibrium location of an atom, and $e^*_{pi\alpha}(\mathbf{K})$ is the conjugate of the projection of the p[th] polarization vector onto the i[th] atom of the unit cell in the α direction. The normal mode coordinates defined above are analogous with the normal coordinates used in electromagnetism. Like normal coordinates in electromagnetism, the vector $\mathbf{e}_p(\mathbf{K})$ is the polarization vector. $e_{pi\alpha}(\mathbf{K})$ is the $i\alpha$ coordinate of $\mathbf{e}_p(\mathbf{K})$. Unlike electromagnetism, the vector $\mathbf{e}_p(\mathbf{K})$ is more than three dimensions; its dimensionality equals three times the number of atoms in a unit cell. Further, the number of mutually orthogonal polarization vectors is also equal to three times the number of atoms in a unit cell, which is the number of degrees of freedom of a given unit cell. The number polarization vectors is

the number of linearly independent ways unit cells in a crystal can vibrate against each other at a given wave vector. In addition, the number of possible wave vectors is equal to the number of unit cells and the crystal Hamiltonian can be thought of as a function of atomic positions or normal mode coordinates. The atomic displacements can be written as functions of the normal coordinates,

$$u_{il\alpha}(t) = \frac{1}{N^{1/2} m_i^{1/2}} \sum_{\mathbf{K},P} e_{pi\alpha}(\mathbf{K}) \exp(i\mathbf{K} \cdot \mathbf{r}_{il}) Q_p(\mathbf{K},t) \tag{2.11}$$

The normal mode coordinates and the atomic displacements are a Fourier transform pair.

By treating the normal coordinates as the independent variables and taking the Taylor expansion with respect to them, the crystal potential energy can be written as

$$\begin{aligned} \Phi &= \frac{1}{2!} \sum_{\mathbf{K}p} \frac{\partial^2 \Phi}{\partial Q_p(\mathbf{K}) \partial Q_p(-\mathbf{K}')} Q_p(\mathbf{K}) Q_p(-\mathbf{K}) \\ &+ \frac{1}{3!} \sum_{\mathbf{K}p,\mathbf{K}'p',\mathbf{K}''p''} \frac{\partial^3 \Phi}{\partial Q_p(\mathbf{K}) \partial Q_{p'}(\mathbf{K}') \partial Q_{p''}(\mathbf{K}'')} Q_p(\mathbf{K}) Q_{p'}(\mathbf{K}') Q_{p''}(\mathbf{K}'') + \ldots \end{aligned} \tag{2.12}$$

In the above expansion only the terms in the second order expansion that have non-zero derivatives have been included. Translational invariance causes the 2nd order derivatives without equal and opposite wave vectors to be equal to zero. Furthermore, eigenvector orthonormality causes 2nd order derivatives with opposite and equal wave vectors, but different polarizations to be zero. This is why normal mode coordinates are completely decoupled from each other. In the harmonic approximation the crystal Hamiltonian is,

$$H = \frac{1}{2} \sum_{\mathbf{K},p} \left[\dot{Q}_p(\mathbf{K}) \dot{Q}_p(-\mathbf{K}) + \omega_p^2(\mathbf{K}) Q_p(\mathbf{K}) Q_p(-\mathbf{K}) \right] \tag{2.13}$$

ω^2 is defined to be the 2nd order derivative appearing in the Taylor expansion with respect to the normal coordinates. The equations of motion of this Hamiltonian result in decoupled normal coordinates with periodic temporal dependencies of frequency ω.

Neglect of the higher order terms results in a model of non-interacting harmonic waves, which is incapable of explaining thermal conduction or expansion even qualitatively. Without the third order terms the phonons never interact (mixed 2nd order derivatives are zero) and without interactions no equilibrium can be obtained and the thermal conductivity would be infinite. Therefore, higher order terms need to be considered. However, the harmonic approximation is an excellent first approximation of the equations of motion.

Consider the 2nd order normal coordinate derivative, using the chain rule and translational invariance it can be rewritten in terms of the 2nd order derivatives with respect to atomic displacements as

$$\omega_p^2(\mathbf{K}) = \frac{\partial^2 \Phi}{\partial Q_p(\mathbf{K}) \partial Q_p(-\mathbf{K}')} = \mathbf{e}_p^{T*} \cdot \mathbf{D}(\mathbf{K}) \cdot \mathbf{e}_P \tag{2.14}$$

where $D(\vec{K})$ is the dynamical matrix and is defined as

$$\mathbf{D}_{3(i-1)+\alpha,3(j-1)+\beta} = \frac{1}{(m_i m_j)^{1/2}} \sum_l \frac{\partial^2 \Phi}{\partial u_{i0\alpha} \partial u_{jl\beta}} e^{i\mathbf{K}\bullet(\mathbf{r}_{jl}-\mathbf{r}_{i0})} \tag{2.15}$$

The matrix is hermitian therefore, it has a full set of orthonormal eigenvectors and those orthonormal eigenvectors are the polarization vectors that are used in the definition of the normal modes. As a result the eigenvalues of the dynamical matrix are the square of the frequency of the normal coordinates. By invoking the Born-Oppenheimer approximation the derivatives in the dynamical matrix can be calculated from an effective interatomic potential. Once dynamical matrices are formed for all wave vectors, the dispersion is calculated by finding their eigenvalues throughout the Brillouin zone.

Most phonon studies of thermal conductivity do not incorporate the use of the full phonon dispersion relationships. While simplified dispersions have had some successes in describing the general trends of thermal conductivity in materials, many models lose the physical details underlying phonon behavior[49]. Simplified dispersion relationships treat optical braches as being at a constant frequency, which results in them having zero group velocity, or simply neglect them. Complex materials can have a significant conductivity contribution from optical branches[6,50], which show much more variation in shape than acoustic branches and cannot be described by simple heuristic arguments. As a result they cannot be modeled adequately without calculating phonon dispersion. Furthermore, the use of simplified dispersions can result in erroneous relaxation times[49] since they can skew fitted constants which are frequently used to estimate relaxation times.

2.5 Phonon Mode Occupancy and Specific Heat

Statistical mechanics is used to calculate the energy and specific heat of a phonon gas. Like a photon the energy of a phonon is the product of Planck's constant and its frequency. The energy of a phonon mode is the product of the number of phonons in the mode and the energy of a phonon in that mode (vacuum energy is neglected). The energy of the entire solid is simply the sum of all phonon mode energies, understanding that the energy of the static lattice is defined to be zero. The heat capacity of the solid is the derivative of the total energy with respect to temperature. In the harmonic approximation phonon frequencies are independent of temperature, so the only temperature dependence of the lattice energy results from changes of the phonon occupancy of the modes.

Phonons have integer spins so like photons they obey Bose-Einstein statistics, therefore the occupancy of a single phonon mode is given by,

$$n = \frac{1}{\exp\left(\frac{\hbar\omega}{k_B T}\right) - 1} \tag{2.16}$$

By taking the derivative of the occupancy with respect to temperature the specific heat of a phonon mode can be calculated. The total specific heat can then be written as,

$$c_v = \frac{1}{(2\pi)^n \rho} \sum_p \int c_p(\mathbf{K}) dK^n \tag{2.17}$$

$$c_p(\mathbf{K}) = k_B \left(\frac{\hbar\omega_p(\mathbf{K})}{k_B T}\right)^2 \frac{\exp\left(\frac{\hbar\omega_p(\mathbf{K})}{k_B T}\right)}{\left(\exp\left(\frac{\hbar\omega_p(\mathbf{K})}{k_B T}\right) - 1\right)^2} \tag{2.18}$$

where n is the dimensionality of the solid. The summation over all wave-vectors in the Brillouin zone has been replaced by an appropriately scaled integral and $c_p(\vec{K})$ is the heat capacity of a single phonon mode. At high temperature the specific heat converges to the classical limit and has a constant value. The preceding analysis is harmonic but the harmonic approximations yield excellent results for the specific heats of many crystals.

2.6 Phonon Velocity

In order to estimate thermal conductivity phonon velocity needs to be calculated. A phonon is a wave-packet centered around some wave vector in wave space so its velocity is the group velocity of the wave and is,

$$\mathbf{v} = \nabla_K \omega \tag{2.19}$$

The above gradient is taken in wave space. The gradient can be calculated two different ways. It can be estimated by calculating the dispersion at different points and then approximating the gradient with finite differences or it can be calculated with the Hellman-Feynman theorem[51]. The finite difference estimation can cause errors because it neglects when two dispersion curves intersect. However, for many solids including zeolites crossing is not common but there are special cases such as nanowires where they may occur frequently. For such cases the Hellman-Feynman theorem can be used. The Hellman-Feynman theorem is a technique for obtaining the derivative of an eigenvalue by taking the derivative of its matrix and projecting it onto the eigenvector of that eigenvalue. The eigenvalues of the dynamical matrix are the squares of the frequency, so the phonon velocity in direction j is[51],

$$v_j = \frac{1}{2\omega}\mathbf{e}^{T*} \cdot \frac{\partial \mathbf{D}}{\partial K_j} \cdot \mathbf{e} \tag{2.20}$$

Because it can handle dispersion crossings without error, the Hellman-Feynman theorem is preferential to a finite difference derivative. If finite differences are used at a point where dispersion curves intersect the phonon speed will be under estimated. Unfortunately, the Hellman-Feynman theorem cannot be readily implemented with commercial software packages. Furthermore, it requires the computation of the phonon eigenvectors, which can become expensive for highly complex materials.

2.7 Phonon Gruneisen Parameters

The phonon Gruneisen parameter is the non-dimensional derivative of phonon frequency with respect to strain. It can be written as[31],

$$\gamma_{ij}(\mathbf{K}, p) = \frac{1}{\omega_p(\mathbf{K})} \frac{\partial \omega_p(\mathbf{K})}{\partial \eta_{ij}} \tag{2.21}$$

The phonon Gruneisen parameter shows how much the frequency of a mode changes when a stain is applied to a lattice. The Gruneisen parameter is the average specific heat weighted phonon Gruneisen parameter and it is written as

$$\gamma_{ij} = \frac{\sum_{\vec{K}p} c_p(\mathbf{K}) \gamma_{ij}(\mathbf{K}, p)}{C_v} \tag{2.22}$$

The Gruneisen parameter is a tensor with different entries corresponding to different strains. It is an indirect measure of crystal anharmonicity and can be used in conjunction with elastic constants to calculate thermal expansion.

2.8 Phonons in Nanowires

Bulk crystals are made up of a single unit cell infinitely replicated and translated in three different spatial directions. This results in the model of a crystal existing everywhere in space. For a nanowire this is a poor mathematical model. Instead a nanowire can be thought of as a unit cell, which includes the entire wire cross section, repeated infinitely in a single direction. Because the crystal lattice of a nanowire is one dimensional it reciprocal lattice is also one dimensional. Hence, the Brillouin zone of a nanowire is a line.

2.9 The Born- Oppenheimer Approximation and Effective Potentials

If the wave function of the entire crystal is known any quantity of interest can be calculated. However, determining the wave-function of a crystal without approximations is impossibly complex to do. For most semi-conductors and dielectrics, including the ones considered in this work, the Born-Oppenheimer approximation is used[47]. For many

materials and material processes the electrons move so rapidly that they can be approximated as shifting instantaneously when the nuclei move. As a result, material energy can be approximated as being solely a function of nuclear coordinates. Hence, a material for which the Born-Oppenheimer approximation is valid can be modeled by an effective potential, independent of electron dynamics. The importance of the Born-Oppenheimer approximation cannot be overstated, without it phonon-dynamics cannot be decoupled from electron dynamics and molecular dynamics would be impossible.

The Born-Oppenheimer approximation allows the use of effective potentials. One common approach to effective interatomic potentials is to use different terms to account for different types of lattice distortions and sum them[52-54]. For this type of potential there is a 2-body term which accounts for bond stretching and compression. Many potentials include a 3-body angle bending term that parameterizes the energy with the respect to the angle between two bonds. Some potentials have a dihedral term that parameterizes the energy with respect to the twist angle between two bonds. A schematic of theses different types of contributions to the potential energy can be seen in Figure 2.7.

Another common class of potentials are bond order potentials[55,56]. Bond order potentials include 2-body bond stretching and 3-body angle terms, but the energy is not the sum of the two. Instead it is a complicated function that correlates the strength of the atomic interactions with the number of atomic neighbors. Depending on the situation one approach may be more appropriate than the other, but in general bond order potentials have the draw back of being substantially more expensive.

Ionic crystals also have long ranged columbic interactions, which can be evaluated using Ewald sums[34] or the method of Wolf[57]. Frequently ions in the lattice are

also given charged massless shells that are attached to the atomic core by a spring to simulate an effective dipole moment[48].

2.10 Summary

A heuristic overview of thermal conduction by phonons was presented. This was followed up by a review of techniques used to calculate thermal conductivity in the phonon picture. Then the underlying theory of phonon dispersion and lattice dynamics was presented. Finally the chapter concluded with an overview of interatomic potentials.

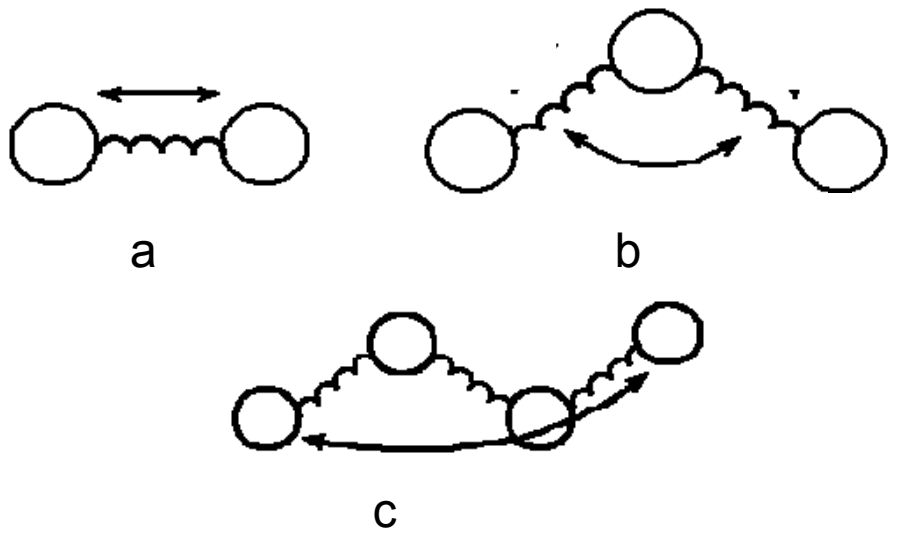

Figure 2.7 Schematic of different contributors to the potential energy of a crystal.
a) bond stretching b) angle bending c) torsional bond twisting. The picture is taken from GSU department of chemistry website.

CHAPTER 3

STRUCTURE, SYNTHESTHIS, AND MEASURED THERMAL CONDUCTIVTY OF ZEOLITE MFI

Zeolites are an important class of materials. This chapter outlines the structural characteristics of zeolite MFI, explains the technique that was used to synthesize it, describes new conductivity measurements, and then concludes with an overview of challenges to accurately modeling its thermal conductivity. It must be noted that the experimental work presented in this chapter was done in collaboration with Yeny Hudiono and a more detailed descriptions of the zeolite synthesis and thermal conductivity measurements can be found in her dissertation[50].

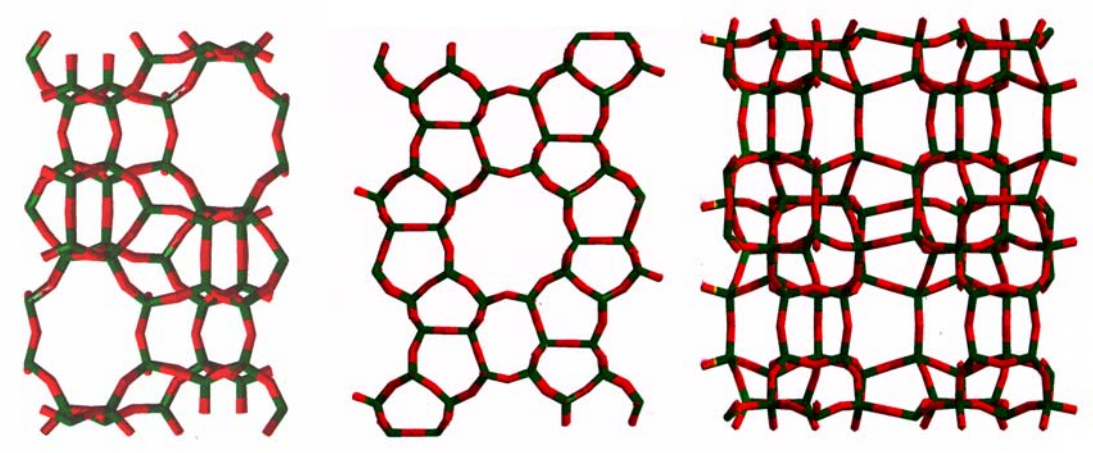

a-direction *b*-direction *c*-direction

Figure 3.1 Structure of zeolite MFI as viewed down crystallographic a, b, c directions.

3.1 Structural Characteristics of Zeolite MFI

MFI has an orthorhombic unit cell with edge lengths of 20.09, 19.74, and 13.14 angstroms. In its purely siliceous form its framework is made up of SiO_2 tetrahedrons. Like many other zeolites, it is highly porous. It has sinusoidal pores with the dimensions of 5.1 Å x 5.5 Å along (100) and a straight channel with the dimensions of 5.3 Å x 5.6 Å along (010). Figure 3.1 shows the unit cell of MFI. Its unit cell is highly complex and has 288 atoms. MFI can be synthesized in an aluminosiliceous form where random silicon atoms, with the constraint that no AlO_2 tetrahedrons can be adjacent to each other[58], are substituted by aluminum atoms. As a result, MFI occurs in different forms that have the same structure but different compositions; this provides a unique opportunity to analyze the effects of composition on the thermal conductivity of highly complex materials

3.2 MFI Synthesis and Sample Preparation

Thick films of MFI are grown using the secondary hydrothermal method[59-61], which is a technique that uses nanoparticles of MFI as nucleation sites to grow a thick films of MFI . Porous (alumina substrates with porosity of 25%) were purchased from Coorstek and polished with SiC paper in order to obtain a smooth surface for deposition of MFI . A clear solution with molar ratio of 1 tetraethylorthosilicate (TEOS) :1 tetrapropylammonium hydroxide : 23 H_2O was hydrothermally a Teflon-lined stainless steel autoclave under rotation, to obtain 100 nm MFI nanoparticles. A MFI nanoparticle dispersion in ethanol was spin-coated on alumina substrates. The coated substrates were placed at an inclined angle (with the seeded side facing downwards) in a Teflon-lined

stainless steel autoclave for hydrothermal synthesis. The secondary growth solutions contained molar ratios of (4−x) TEOS: x Al:0.9 tetrapropylammonium bromide (TPABr) : 0.9 KOH: 940 H_2O, with $0<x<0.25$. Potassium aluminate solution was prepared by hydrolyzing aluminum powder in KOH, TPABr, and water solution for 1 h. Potassium silicate was prepared by mixing TEOS in KOH, TPABr, and water solution for 1 h, and then both solutions were mixed together. The films were rinsed with hot de-ionized water, dried, and calcined in air at 500 °C for 6 hours. The films were then characterized by x-ray diffraction (PANalytical X'Pert Pro, Cu K ALPHA) to obtain the film orientation. The films were first polished with SiC paper then sequentially polished with alumina polishing suspensions. The film roughness was characterized by atomic force microscopy (AFM) using the contact mode technique. The film thicknesses and compositions were characterized by a scanning electron microscopy equipped with energy dispersive spectroscopy. Pictures of the siliceous MFI film can be seen in Figure 3.2.

3.3 MFI Thermal Conductivity Measurements

The thermal transport properties of MFI zeolite films were characterized using the three-omega technique[62,63]. The three omega technique uses a four point probe metal line as a thermometer and a heater. An alternating current through the heater at frequency ω causes Joule heating to occur at a frequency of 2ω this in turn induces a harmonic signal at 3ω, which is caused by the temperature dependence of the heater's resistivity. As a result, the thermal conductivity can be deduced from the 3ω signal because the 3ω signal is dependant on the periodic temperature fluctuations in the heater which in turn are dependant on the thermal properties of the film. More details about the

experimental setup and data analysis used in the three-omega technique can be found elsewhere[62,63].

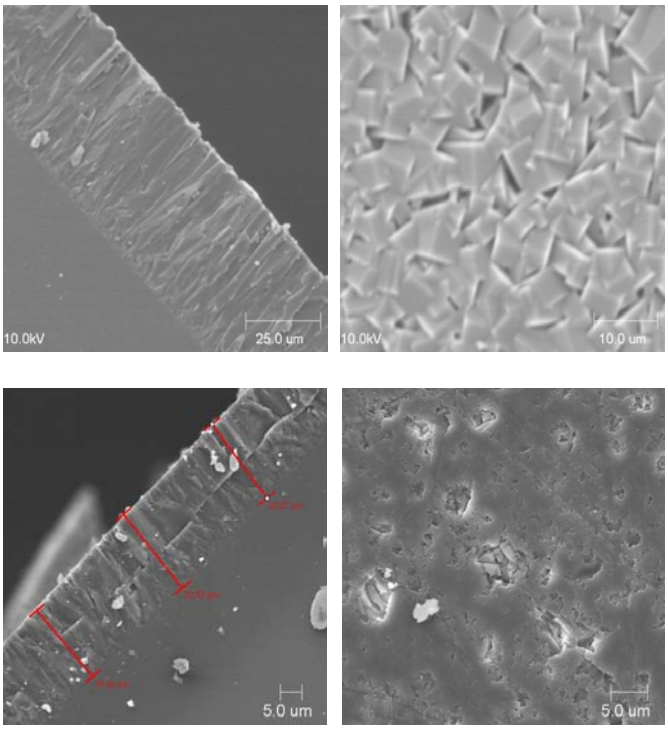

Figure 3.2 Unpolished and polished MFI films. The top two pictures are of the unpolished pure-silica MFI film and the bottom two pictures are the polished pure-silica MFI film

To measures the thermal conductivity of the MFI films a four point probe metal heater was fabricated on the film surface by evaporation of titanium and gold layers through a shadow mask. The thickness of the titanium layer was 30 nm and the thickness of the gold layer was 160 nm. An alternating current signal of amplitude 5 V was applied to the metal heater. Both the in-phase and out-of-phase response of the third harmonic voltage over a frequency range of 75–2000 Hz were employed to analyze the thermal conductivity of the MFI zeolite films. The measurements were performed at temperatures between 150 and 450 K in a vacuum cryostat (~10^{-8} Torr). The three-omega voltage

responses were obtained and used to calculate the thermal conductivity. The magnitude and phase of the three-omega voltage are directly related to the temperature response of the metal line, which is a function of the thermal properties of the underlying material. The thermal conductivity was deduced by a least-squares fit of a 2-D analytical solution for a periodic heat source on a multilayer-film-on-substrate system[62]. The thermal conductivity of the substrate was measured separately using the same methods and was then input as a parameter to fit MFI's conductivity. The measured conductivities can be seen in Figure 4.4 of the next chapter.

3.4 Challenges in Modeling the Thermal Conductivity of Zeolites

Computational approaches have primarily relied on classical molecular dynamics simulations[7,8], which cannot account for quantum effects. Deviations from classical behavior of thermal properties are particularly large for zeolites. This occurs because zeolites have many high frequency phonons, which make substantial contributions to the thermal conductivity and high frequency phonons only behave classically at very high temperatures. When conductivity increases with temperature, which MFI does even at moderately high temperatures, quantum mechanical effects cannot be neglected. Conductivity is dependant on phonon relaxation time, which can only decrease with increasing temperature, phonon velocity, which to a rough approximation remains constant with temperature, and phonon specific heat. Classically phonon specific heat is roughly temperature independent but quantum mechanically it increases with temperature[64]. Therefore the increase in thermal conductivity with temperature demonstrates that quantum effects are important because the quantum mechanical

specific heat is the only quantity that thermal conductivity is dependant on that increases with a rise in temperature.

If a material's conductivity continues to rises at moderate temperatures the traditional phonon conductivity modeling approach of Klemens[15], Callaway[16], and Holland[17] cannot be used. At moderate temperatures the low frequency acoustic phonons have already reached the classical limit, so their contribution to the conductivity is decreasing. This implies that the optical phonons, which are not in the classical limit, are contributing substantially to the conductivity; otherwise conductivity would decrease with increasing temperature. In chapter 2, it was explained that phonon models which use the Debye model for phonon dispersion can only be used when long wave length acoustic phonons are dominating the conductivity. Murashov[9], attempted to model the thermal conductivity of zeolite LTA with a Klemens like model. However, the calculation was found to be unrepeatable. The inabilities of molecular dynamics and traditional relaxation time modeling to calculate the thermal conductivity of zeolite MFI necessitates a new modeling approach which is applicable to highly complex crystals like zeolite MFI.

MFI's complexity makes it particularly challenging to model its thermal conductivity in a way that is both computationally feasible and physically sensible. An outright calculation of phonon relaxation times is prohibitively expensive and will continue to be for some time. Furthermore, relaxation time is not the only expensive part of a conductivity calculation and many aspects of an MFI conductivity model need to be approximate.

3.5 Summary

The structure of zeolite MFI, which has many features common to all zeolites, has been described. This was followed by a brief overview of the experimental techniques used to synthesize and measure the conductivity of zeolite MFI. Finally, the short comings of previous zeolite conductivity modeling and the challenges of new zeolite conductivity modeling were discussed.

CHAPTER 4

MODELING THE THERMAL CONDUCTIVTY OF ZEOLITE MFI

As explained in the last chapter zeolite thermal conductivity cannot be calculated accurately with molecular dynamics because it's purely classical and zeolite thermal conductivity exhibits strong quantum effects. Further, previous relaxation time models are inapplicable because they assume that long wave length optical phonons are the dominant heat carrier, which is not the case for zeolites and other highly complex materials[6,12,65,66]. Therefore, a new modeling paradigm for highly complex porous materials is needed. The experimental data collected for this study is an invaluable tool for understanding thermal transport and developing new modeling methodologies not only for zeolites but also for complex crystals in general. Furthermore, because the data is collected on MFI with different Si/Al ratios this study has a unique opportunity to analyze the effects of composition and defect scattering on highly complex materials.

In this chapter Zeolite MFI is used as case study to develop a more general phonon relaxation time framework to model the thermal conductivity of highly complex crystals. The new methodology developed here is used to study the thermal conductivity of Zeolite MFI as a function of the Si/Al ratio. The full phonon dispersion of the material is used instead of simplified forms that have been used in previous relaxation time models. The first step in the methodology is to determine the equilibrium crystal structure of zeolite MFI. This is done by inputting the estimated atomic positions (from spectroscopic data) and an effective interatomic potential into an energy minimization algorithm. The equilibrium atomic positions are those for which the potential energy is at

a local minimum. Once the equilibrium positions are known the phonon dispersion is calculated. Then phonon velocity and specific heat are calculated from the dispersion. Next the relaxation time is approximated using a semi-quantitative functional form that relies on fitted constants. Finally, the relaxation time expression, phonon velocity, and specific heat are put into Equation 2.1 and the fitted constants are obtained by fitting Equation 2.1 to the experimental data.

4.1 Interatomic Potential for Zeolite MFI

Before any calculations can be done an interatomic potential needs to be chosen. For MFI the Catlow[53] potential is used because of its ubiquity and many successes. It includes a Buckingham term for dipole-dipole interactions for O-O and Si-O bonds, a three body term for angle bending of the SiO_2 tetrahedrons, a Coulombic term resulting from the polarity of Si-O bonds, and a core-shell model for Oxygen polarizability.

4.2 Determination of the Unit Cell

Once the potentials have been picked the equilibrium atomic positions need to be determined. This is done by using good initial guesses for the desired crystalline structures and then minimizing the energy of the crystalline structure with respect to the atomic coordinates. For MFI structures with different Si/Al ratios need to be constructed. To create them random Si atoms are replaced by Al atoms, with the constraint that no two Al sites can be adjacent as dictated by Loewenstein's rule[58]. When a Silicon atom is replaced by an Aluminum atom the atomic charge of the unit cell goes down by one, so a proton is added to the unit cell to make it electrically neutral. The proton is placed in a pore, which is one of the most electronegative regions of the crystal, and bonded to an Oxygen atom that is bonded to an Aluminum atom. The force field used for

aluminosiliceous MFI has all the terms used in siliceous MFI in addition to a Buckingham term for Al-O dipole-dipole interaction, an angle bending term for AlO2 tetrahedrons, and a Morse potential for the O-H bond.

In order to model thermal conductivity within the framework of phonon theory a periodic unit cell is needed. One unit cell (of size ~5360 Å3 and containing 288 atoms) is used for the computations, since larger unit cells are computationally too demanding. Crystal structures with Si/Al ratios of 95, 47, and 31 were created and used to describe the behavior of the experimentally generated Si/Al ratios of 82, 36, and 26. This approximation is made in an obviously consistent manner and does not lead to any loss of understanding of the phonon physics This will lead to a slight overestimation of phonon velocity but the overestimation is consistent and the goal is not a perfect calculation but to elucidate trends and understand phonon physics. The use of one unit cell will also introduce artificial periodicity but this should have minimal effects on the model because the following. An impurity will only affect local bonding because dipole-dipole interactions and the disturbance in the electric field, which is a small dipole moment caused by the proton and Aluminum atom, are both short ranged. Furthermore, only small amounts of Al are being considered and the unit cell of MFI is fairly large. Therefore, the different impurity sites should be largely independent of each other.

4.3 Energy Minimization of the Crystal

The General Utility Lattice Program[67] is a commercial lattice dynamics software package, which can be used to minimize crystal energy and calculate phonon dispersion. For zeolite MFI it was used to do both these things. During the energy minimizations, the fractional coordinates of all 288 atoms in the MFI unit cell are allowed to relax and the

unit cell parameters are left constant at the values obtained from the crystal structure. Newton–Raphson and rational function optimization minimization techniques are used. The potential energy surface is complicated and has many saddle points. Therefore, care must be taken when analyzing the results. The eigenfrequencies reveal if a local minimum has been reached. If all the phonons frequencies are real the dynamical matrix is positive definite, which implies the positive definiteness of the Hessian matrix. The structures are also examined visually to verify their reasonableness.

4.4 Phonon Spectra of Zeolite MFI

The full anisotropic phonon dispersions for all 864 branches are calculated across the entire Brillouin zone. The dispersions are calculated by evaluating the square roots of the dynamical matrix eigenvalues across an evenly spaced grid of 1000 points that spans the positive octant of the Brillouin zone, this is done using GULP. The effect of aluminum configurations is checked by calculating the dispersion for two structures with the same Si/Al ratios but different aluminum atom locations. The resulting dispersions are only weakly dependent on the configuration of the aluminum atoms. Figure 4.1 shows the dispersion in the (1 0 0) direction for an acoustic and optical branch.

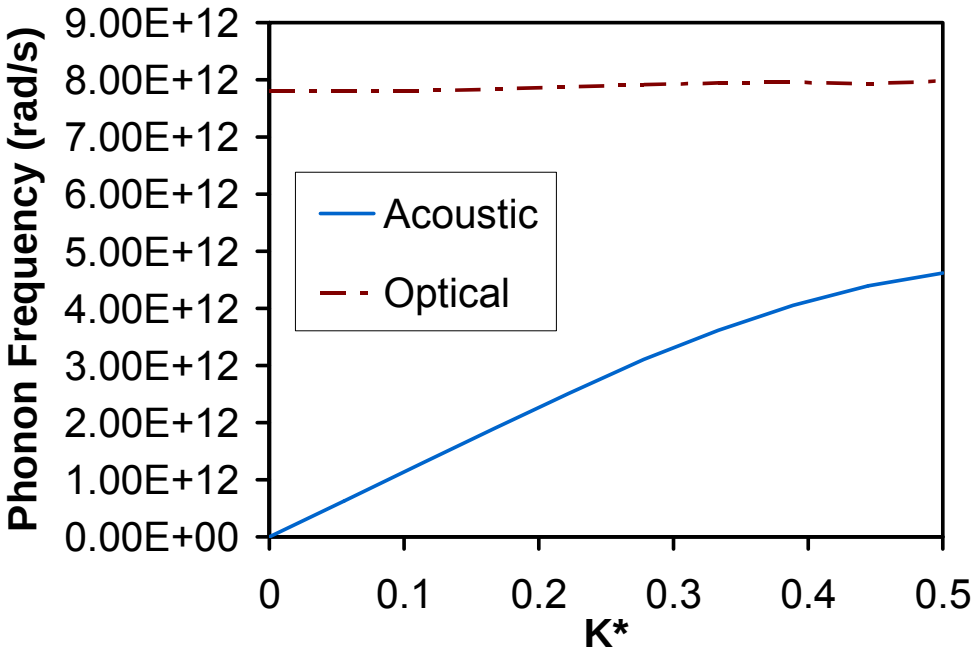

Figure 4.1 Phonon dispersion for siliceous MFI along the (1 0 0) direction of the Brillouin zone. The x-axis is the non-dimensional position along the (1 0 0) edge of the Brillouin zone. The non-dimensional coordinates shown start at the center of the zone and go to the zone edge.

The group velocities are calculated by taking the gradient of the dispersions. The gradient is approximated by finite differences of the dispersion in the Brillouin zone. This may cause some error when dispersion branches cross. However, this error is small because group theory reveals that with the exception of directions of symmetry in the Brillouin zone phonon band crossings are unlikely to occur[68]. In addition, MFI is a low symmetry crystal so there are not many symmetric directions in the Brillouin zone. As a result the error introduced by using finite differences should have minimal qualitative effects. Further, many highly complex crystals have more atoms in a unit cell then MFI

so for these crystals using the Hellman-Feynman theorem is expensive. Figure 4.2 shows phonon velocities in the (1 0 0) direction for the dispersions shown above.

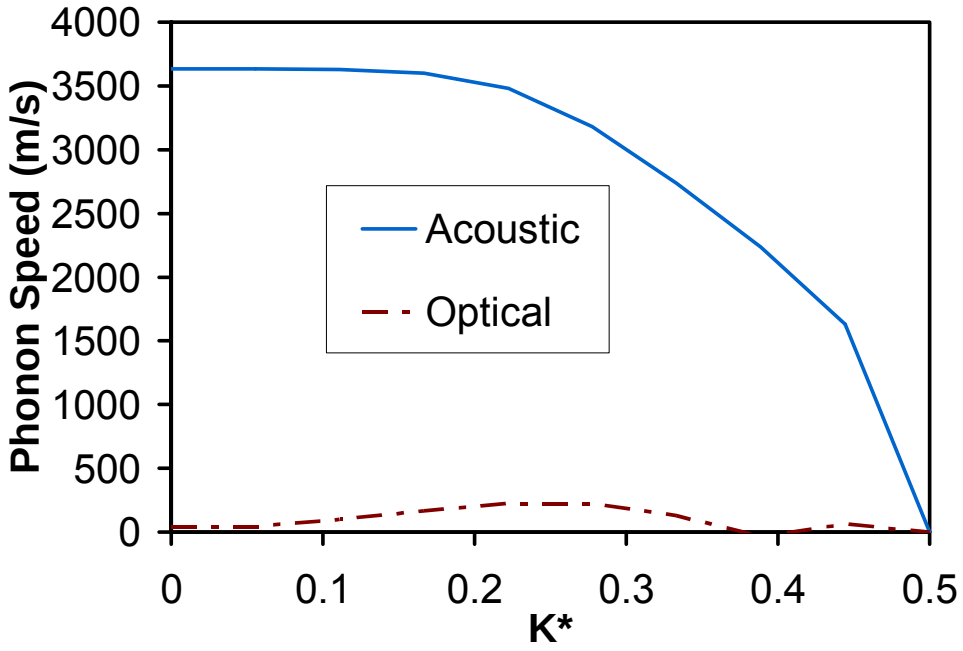

Figure 4.2 Phonon speeds of the same phonon branches shown in Figure 4.1. The acoustic phonon velocity goes discontinuously to zero at the zone center. This is not shown on the graph.

Notice the optical phonons are much slower than the acoustic ones; this is typical of optical phonons in general. However, MFI has 861 optical branches and only three acoustic branches as a result the numerous optical branches add up and contribute substantially to the thermal conductivity.

4.5 Phonon Relaxation Time in MFI

A critical issue in modeling the thermal conductivity of crystals is the calculation of the phonon relaxation lifetimes that result from different phonon scattering mechanisms operating in the material. As mentioned earlier, there is no clear unambiguous way to calculate the relaxation time. The approach used here is to neglect normal processes. This is done because normal processes do not directly contribute to the thermal resistance and in Zeolite MFI and silicates in general[14] it is expected that normal scattering events will be far fewer than umklapp events, even at moderately low temperatures. Therefore, the approach used here for MFI is equivalent to the SMRT approximation, which assumes that phonon relaxation time is the same as phonon lifetime.

In theory, phonon lifetime can be calculated from the Fermi scattering equation[22,37]. However, this calculation is extremely expensive for a simple material, and all but impossible for a complex material such as MFI. There have also been molecular dynamics studies that explicitly calculate phonon lifetimes in simple crystals[45,69], but this approach requires a large number of simulations with varying system sizes in order to adequately sample the Brillouin zone. The size and complexity of the MFI unit cell precludes the computational feasibility of this approach. As a result, semi theoretical expressions are used to estimate the relaxation times[15,20,21,41].

The three processes considered in the present thermal conductivity model are umklapp phonon-phonon scattering, boundary scattering, and point defect scattering. The umklapp scattering term used here is

$$\tau_U^{-1} = B\omega^2 T e^{-\frac{\theta_D}{3T}} \tag{4.1}$$

B is a fitted constant that is ascertained by fitting the thermal conductivity model to experimental data and θ_D is the Debye temperature. The above expression was not originally developed for materials as complex as MFI. Its use is more appropriate with quartz or another dense silica polymorph. However, there are no available phonon-phonon relaxation time expressions that are more appropriate for MFI. To compensate for this a boundary scattering term is added because MFI can be thought of as a dense silica polymorph with large pores in it. The boundary scattering term also include scattering from stacking faults grain boundaries and other planar defects. The boundary scattering term is[35],

$$\tau_B^{-1} = \frac{v}{l_{eff}} \tag{4.2}$$

l_{eff} is the effective distance between boundaries and interfaces a phonon can scatter off. It depends on the shape and size of domains, and interfacial reflectivity and is also treated as a fitted constant. It is the only scattering term used here that is not derived from time dependant perturbation theory. Ziman[35] derived it directly from the Boltzmann transport equation. The point defect scattering term is[22]

$$\tau_D^{-1} = A\omega^2 g(\omega) \tag{4.3}$$

A is a fitted constant and g is the phonon density of states. A could theoretically be calculated if enough structural information for the crystal were known. However, it requires knowledge of the exact location of everything single defect in every single unit cell of the entire crystal to calculate. Further, with exception of isotopic scattering, if all the required information were known it would still be prohibitively expensive to calculate for MFI. The above expression is used to estimate phonon scattering off intrinsic

defects in the siliceous MFI, and more importantly the scattering of phonons off aluminum atoms in the aluminosiliceous samples. Its use is predicated on assuming that the aluminosiliceous MFI can be thought of as a perturbation of siliceous MFI. For the MFI compositions considered here only one, two, or three silicon atoms are replaced with aluminum atoms. Further there are 288 atoms in a unit cell, so the structures are similar. Hence, the aluminosiliceous MFI can be thought of as a perturbation of the siliceous MFI.

Once all the phonons scattering mechanisms have been identified, the total relaxation time can be calculated from Matthiessen's rule which gives an overall scattering rate of

$$\tau^{-1} = \tau_U^{-1} + \tau_B^{-1} + \tau_D^{-1} \tag{4.4}$$

Matthiessen's is commonly used[15,22,35] and should introduce little or no error into the calculation.

4.6 Calculating the Specific Heat

The specific heat is calculated for siliceous MFI and aluminosiliceous MFI with Si/Al ratios of 95,47, and 31 by inputting each sample's calculated dispersion into Equation 2.17. The specific heat is identical for all samples and implies that the phonon frequencies change very little from sample to sample. This is not surprising because the composition changes very little form sample to sample.

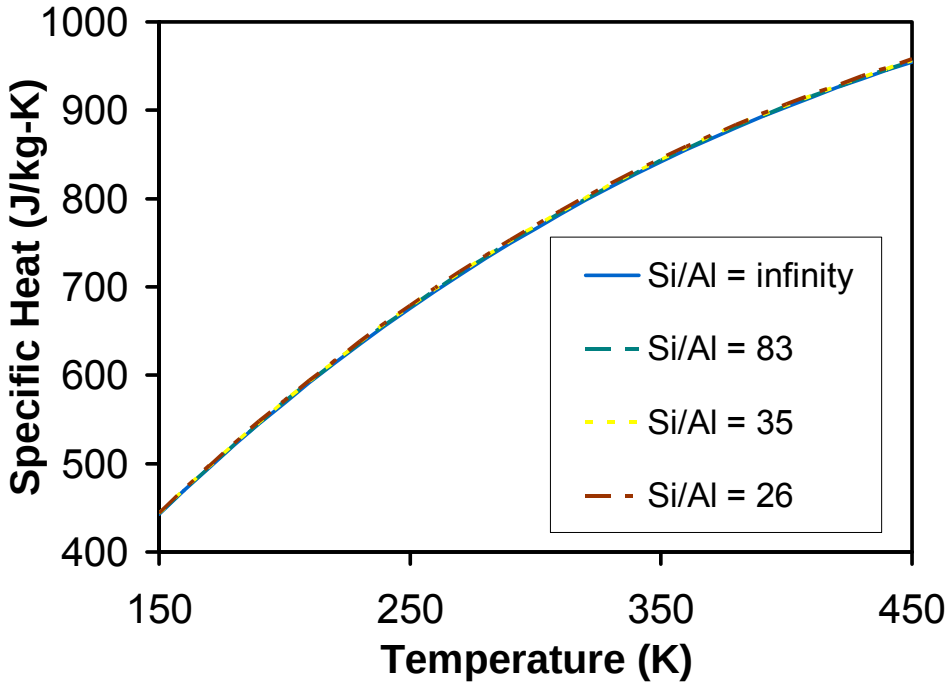

Figure 4.3 Calculated specific heat of MFI with different Si/Al ratios.

4.7 Calculating the Conductivity

By combining Equations 2.1, 2.18, 2.19, 4.1, 4.2, and 4.3 the expression used to calculate the thermal conductivity can be written as

$$k_j = \frac{1}{(2\pi)^3}\sum_p \int k_B \left(\frac{\hbar\omega_p(\vec{K})}{k_B T}\right)^2 \frac{\exp\left(\frac{\hbar\omega_p(\vec{K})}{k_B T}\right)}{\left(\exp\left(\frac{\hbar\omega_p(\vec{K})}{k_B T}\right)-1\right)^2} \left(\nabla_K \omega_p(\vec{K})\cdot \hat{j}\right)^2 \times \left(B\omega^2 T e^{\frac{-\theta}{3T}} + \frac{\left|\nabla_K \omega_p(\vec{K})\right|}{l_{eff}} + A\omega^2 g(\omega)\right)^{-1} dK^3 \quad (4.5)$$

As mentioned in the last chapter, thermal conductivity data as been collected at temperature from 150 to 450 K for four different MFI samples with four different Si/Al ratios. The above equation is simultaneously fitted to all the experimental data for all the samples. B is the same for all samples because the added aluminum defects are treated as perturbations so the phonon-phonon relaxation time is the same for all samples. The pore structure is the same for all samples and l_{eff} indicative of phonons scattering off planar defects and pores, as a result l_{eff} is the same for all MFI compositions. A is different for different samples because it is dependant on aluminum content. As a result, a total of only six fitted constants are used to fit all the data. The fit is done using non-linear least squares regression. Unlike linear regression it is unable to fully explore the entire space of all parameter values. To insure the full parameter space is explored, the fit was repeated for many different input parameter values and it was found that the obtained fit is the only reasonable one.

Because the dispersion is calculated for each sample, one complication that arises from the perturbation treatment of the phonon-defect scattering is the problem of double counting. This occurs because the umklapp scattering rate is the same for all samples but different dispersions are input into the umklapp scattering rate for the different samples. However, the error introduced by this will be minuet because the phonon frequencies in the different samples do not differ much from each other. The use of the same l_{eff} for all samples does not lead to double counting because the boundary scattering term is based on the Boltzmann transport equation and not perturbation theory. Figure 4.4 shows both the measured and calculated thermal conductivities.

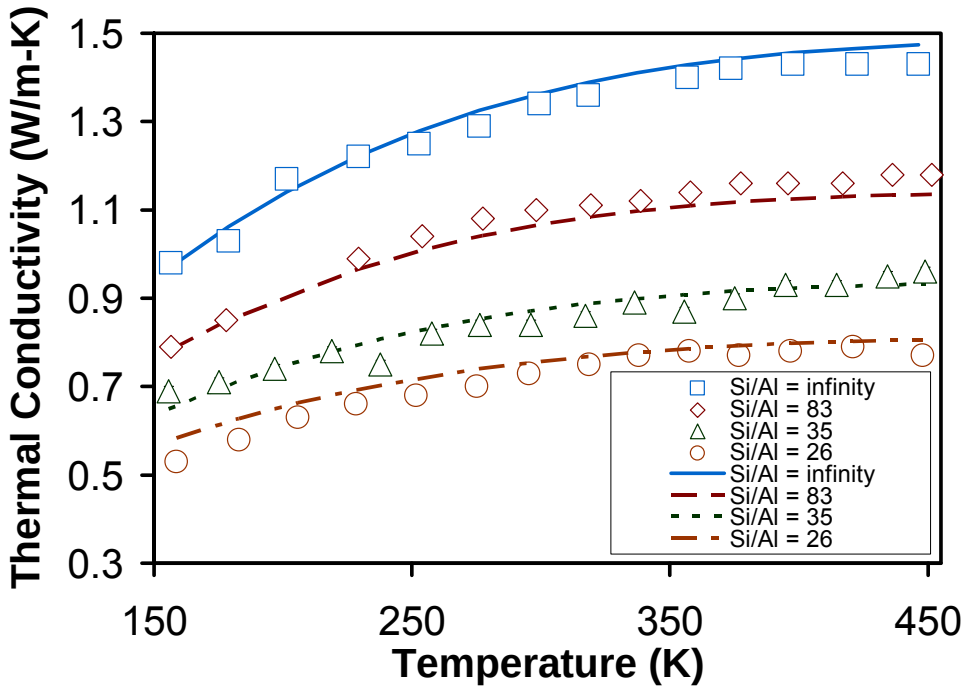

Figure 4.4 Measured and calculated thermal conductivity of MFI with different Si/Al ratios.

Considering the small amount of parameters used the obtained fit is of excellent quality. The values for the fitted parameters are listed in Table 4.1. The boundary scattering term (with a fitted l_{eff} of 4.8 nm) makes by far the strongest contribution of the three phonon scattering mechanisms and limits the absolute value of the thermal conductivity. The obtained value of l_{eff} is worthy of more detailed discussion. Several authors report the existence of sub-100-nm domains in zeolite crystals[70,71]. An upper limit on the domain size is estimated from XRD[50], performed on the MFI samples used here, as (100 nm) by the Scherrer relation which uses the full width at half maximum of the XRD peaks. However, the Scherrer domain size (100 nm) is much larger than the fitted l_{eff} and is unlikely to limit the propagation of phonons at nanometer length scales. Furthermore, the

MFI structure is inherently free of pore stacking faults that might also act as phonon scattering boundaries. The high quality of the obtained fit strongly implies that the temperature-independent boundary-like scattering mechanism arises from the interaction of the lattice vibrations with the pore network, which disrupts long-range lattice vibrations. The periodicity of the pore structure in MFI is about 1.5 nm and the crystallographic pore size is about 0.9 nm. Heat carriers would thus have a mean free path that is determined by the length scale of the pore network. From the point of view of real-space visualization of thermal transport (as opposed to the present reciprocal-space approach), the presence of nanoscale voids would impede the atom-to-atom transfer of heat energy at the surfaces of these voids, since this heat energy must be either reflected back from the void/pore or be channeled around it. Recently, similar arguments based upon the results of molecular dynamics simulations have been advanced to qualitatively explain the thermal conductivity of nanoporous metal-organic frameworks[65].

The substitution of aluminum atoms changes the shape of the thermal conductivity curve. This occurs because higher frequency phonons scatter off of aluminum defects much more often then low frequency ones. As a result, defect scattering suppresses high frequency phonon thermal conductivity more than low frequency phonon thermal conductivity. Therefore, as higher frequency modes become excited they contribute less to the thermal conductivity than they would in siliceous MFI and this causes the thermal conductivity to change less.

Despite the quantitative success and physically reasonable qualitative explanations that the current relaxation model provides, a more realistic relaxation model is still needed. The need to heuristically use a boundary scattering term that dominates

the thermal conductivity when there is no indication of large amounts of planar defects implies that a superior umklapp scattering term is needed. If the umklapp scattering expression used here were fully adequate it would automatically include the boundary like scattering.

The fact that the thermal conductivity continues to rise at the temperatures shown, implies the substantial contribution of the optical modes to the thermal conductivity. This is because even at 150 K all the acoustic phonons in MFI have reached the classical limit, so their thermal conductivity at the temperatures shown can only decrease with increasing temperature. The approach adopted here is to treat thermal transport in the diffusive regime. However, there is a possibility that the unsual temperature dependence of MFI's thermal conductivity may be caused by phonon hopping[72] and not just the importance of optical phonons. It is interesting to note that small amounts of Al can drastically change the thermal conductivity even at high temperatures, where defect scattering is typically unimportant[19,21,27]. MFI with a Si/Al ratio of 26 has an average of 3.5 silicon atoms replaced with aluminum ones per unit cell. MFI has 288 atoms in a unit cell, so the change in composition is very small, yet even at the high temperature of 450 K, its thermal conductivity is half that of siliceous MFI.

Even though boundary scattering dominates the thermal conductivity, defect and umklapp scattering are still important. The mean free path for all samples is shown in Figure 4.5. It was calculated by averaging the mean free path of all phonon modes with modal thermal conductivity used as a weighting function.

For the siliceous sample the boundary scattering term is the only important scattering mechanism at 150K, and the small A value for this sample implies that point

defect scattering is not important at any temperature. However, as the sample gets hotter the temperature dependant umklapp scattering term gains in strength and cause the mean free path to drop.

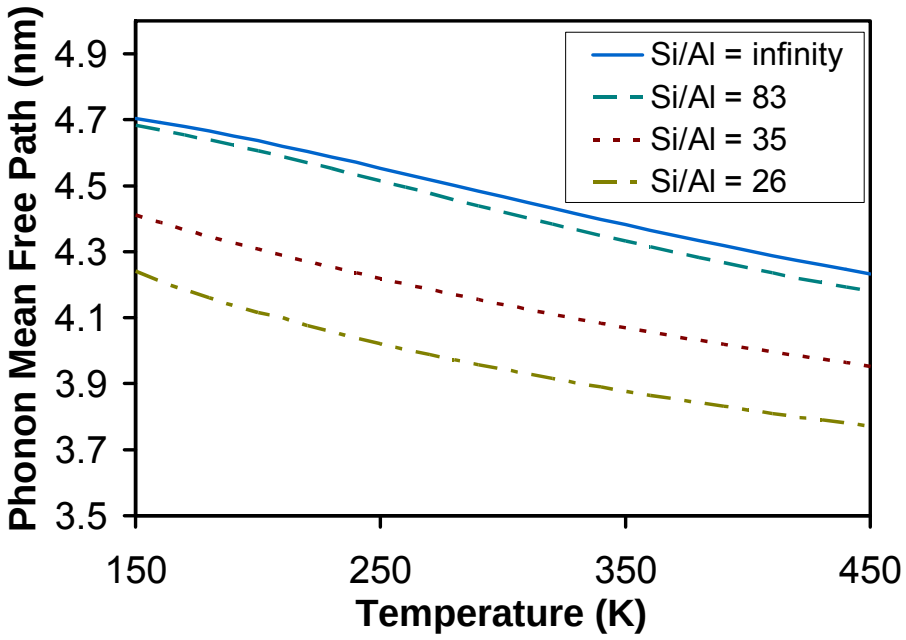

Figure 4.5 Modal thermal conductivity weighted phonon mean free path for all MFI samples.

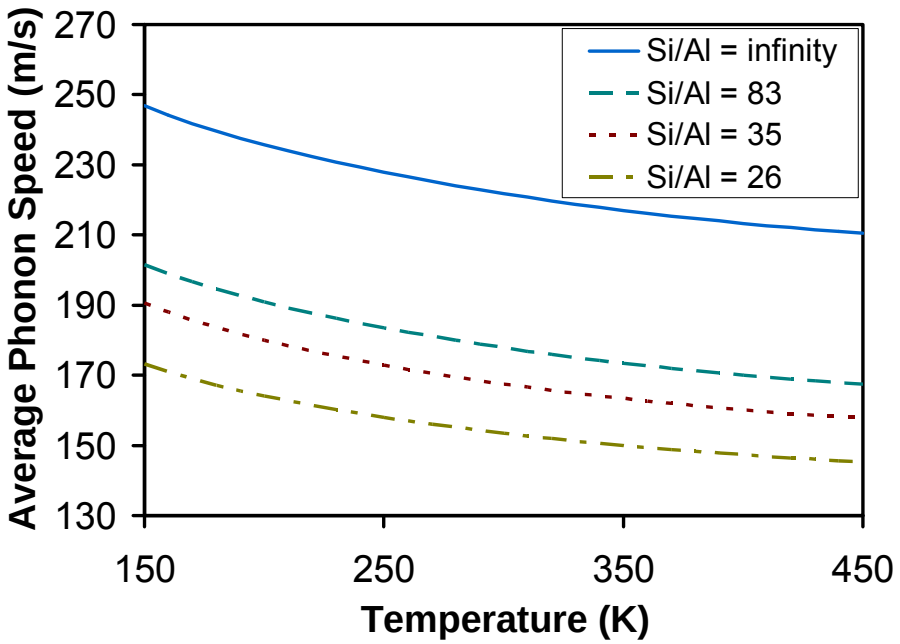

Figure 4.6 Average phonon speed in the (1 0 1) direction. Modal specific heat has been used as a weighting function

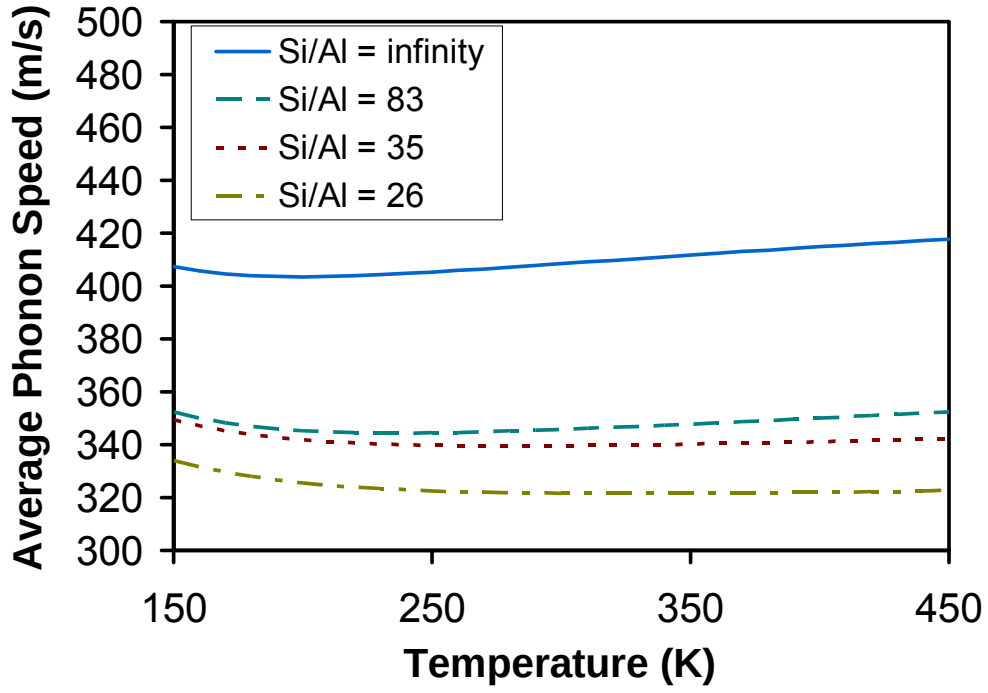

Figure 4.7 Average phonon speed in the (1 0 1) direction. Modal phonon conductivity is used as a weighting function.

The mean free path also drops with increasing temperature because higher frequency modes become important in the average and they experience much more umklapp scattering than the low frequency modes. With increasing Aluminum content the mean free path continues to drop. However, the modest decrease in mean free path caused by the substitution of silicon atoms with aluminum ones cannot explain the large drop in thermal conductivity. Further, specific heat is independent of aluminum content so the only possible explanation is that introducing aluminum defects causes phonons to slow substantially.

Figure 4.6 shows the modal phonon specific heat weighted average phonon speed in the (101) direction of MFI. The averaging is done by using the specific heat of each phonon mode as a weighting function. This allows a truer picture of the average speed of phonons that contribute to thermal conductivity because high frequency phonons, which do not contribute to the thermal conductivity much, have small modal specific heats so the weighting ensures they don't contribute much to the average phonon speed. Despite the small changes in composition the drop in phonon velocity is substantial. This is a feature that is unique to crystals where optical phonons dominate the thermal conductivity. This happens because even though the frequencies change little with aluminum content small changes to the relatively flat optical branches can lead to large relative changes in the small optical phonon velocities. By comparing Figures 4.4, 4.5 and 4.6 it becomes apparent that consideration of phonon slowing is essential to consistently modeling the effects of point defects on complex crystals. Typically thermal

conductivity models only account for the changes of scattering rates that defects cause and not the changes in phonon speed

The modal conductivity weighted averaged phonon speed is shown in Figure 4.7. Ideally it is a more accurate measure of the speeds of the phonons that contribute the most to the thermal conductivity than specific heat weighted phonon speed. However, unlike the specific heat weighted average phonon speed it is approximate because it is dependant on the distribution of scattering rates amongst phonon modes, which may have some error due to the approximate nature of the relaxation time calculation. However, it gives a more accurate picture of how phonon slowing affects thermal conductivity. The average speeds are higher than in the specific heat weighted speeds because higher frequency phonons tend to move slower, scatter more, and contribute to the conductivity less than low frequency phonons. At higher temperatures the average speed decreases because the temperature dependant umklapp scattering increase in strength which cause high frequency phonons to scatter more.

4.8 Error Analysis

The sensitivity of the fitted parameters is analyzed by calculating their 95% confidence intervals. The confidence intervals are expressed as the percent of the values of the fitted parameters and are shown in Table 4.1. They are large; however the defect scattering term in the MFI sample with no aluminum barely affects the thermal conductivity. Its lack of significance causes the Jacobian of the fitted parameters to be nearly singular, which results in large error prone confidence intervals. To circumvent this problem the fits are redone without a defect scattering term for the MFI sample with no aluminum. The new fitted constants and their confidence intervals are shown in Table

4.2. The thermal conductivity fits with the new parameters are not shown but they are similar to the original fits. The constants from the new fits are similar to those of the original fits. The confidence intervals of the second fit directly reflect the importance of the different scattering terms to modeling the conductivity. The defect scattering constant for the Si/Al = 83 sample is particularly large. This may occur because of uncertainties in the aluminum content of the samples, inaccuracies in the assumed functional form of the scattering rates, or because the small amount of defect scattering in the sample is difficult to accurately fit because of noise in the data.

Table 4.1 Fitted phonon scattering model parameters for MFI films. Umklapp parameter B and effective domain size l_{eff} are held constant across all the samples whereas A varies with Al content. Confidence intervals are expressed as the percent of the fitted constant they correspond to.

	Fitted Constants	95% confidance interval
B (s/K-rad^2)	7.44E-21	49.79
l_{eff} (m)	4.80E-09	19.67
A Si/Al = Inf(s/rad^2)	7.00E-31	896.85
A Si/Al = 83 (s/rad^2)	7.42E-31	808.52
A Si/Al = 35 (s/rad^2)	4.43E-30	193.54
A Si/Al = 26 (s/rad^2)	8.70E-30	122.70

Table 4.2 Second set of fitted phonon scattering model parameters for MFI films. Umklapp parameter B and effective domain size l_{eff} are held constant across all the samples whereas A varies with Al content. For this fit no point defect scattering term is included for the Si/Al = infinity sample. Confidence intervals are expressed as the percent of the fitted constant they correspond to.

	Fitted Constants	95% confidance interval
B (s/K-rad²)	1.07E-20	25.88
l_{eff} (m)	4.80E-09	3.09
A Si/Al = Inf (s/rad²)	0.00E+00	not fitted
A Si/Al = 83 (s/rad²)	8.66E-31	95.93
A Si/Al = 35 (s/rad²)	5.52E-30	24.57
A Si/Al = 26 (s/rad²)	9.48E-30	22.53

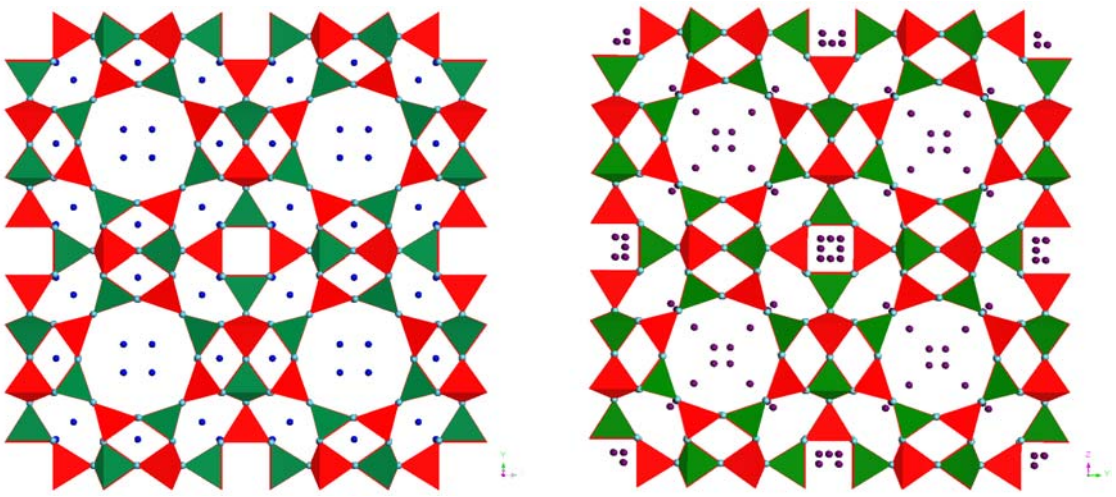

Figure 4.8 The crystal structures of (a) sodium LTA[73] , and (b) potassium LTA[74]. The dark blue and purple dots are possible cation locations and the green and red tetrahedrons are silicon and aluminum tetrahedrons.

4.9 Application of Modeling Methodology to Zeolite LTA

The new modeling paradigm that has been developed is now extended to zeolite MFI, so the effect of non-framework cations on conductivity can be analyzed. Figure 4.8 shows the unit cell of zeolite LTA. The unit cells shown in Figure 4.8 are actually supercells made up of four primitive unit cells. Like all zeolites LTA is made up of silicon and aluminum tetrahedrons. LTA has a Si/Al ratio of one. Because of Lowenstein's rule, ideal LTA has perfectly ordered silicon and aluminum atoms. Aluminum has a smaller charge than silicon so non-framework cations become embedded in the pores so the crystal will be electrically neutral. Na-LTA, K-LTA and Ca-LTA were synthesized using the secondary hydrothermal method and had their conductivities measured using the three-omega technique (for more details see Hudiono[50]).

The LTA unit cell has 96 Aluminum atoms so the sum of charges from all non-framework cations is 96. Sodium and potassium ions have a charge of +1 and calcium ions have a charge if +2, so Na-LTA and K-LTA have 96 cations and Ca-LTA has 43. For each type of LTA there are far more cation sites than cations as a result zeolite LTA has a substantial amount of disorder. Because of the disorder four primitive lattice cells are used to make a unit cell to perform calculations on. It would be ideal to use even more primitive cells to get a better representative unit cell but it would be too expensive.

The unit cells used for the calculation are made by taking spectroscopic data, which gives cation site location and occupancy, from the literature[73-75], and then placing cations randomly at different cation cites according the experimental occupancy. For some sites there are rules where if site A is occupied site B cannot, so the sites were

randomly picked in a way to satisfy such constraints. To insure that the unit cells used appropriately represents the material three different unit cells with random cation sites were made for each LTA type. For each LTA type the density of states were calculated and compared for the three different representative unit cells with different cation locations. For all types of LTA the density of states was almost exactly the same for all three representative unit cells, so four primitive cells should be enough to represent the disordered material.

After the cation locations were selected the energy of the entire unit cell (both the framework and the cations) is minimized. The same effective potential that is used for MFI is used for all three types of LTA. Buckingham potential terms for the dispersive interaction of the cations with the framework[54] are also included. The same methodology used to model MFI is used to model LTA.

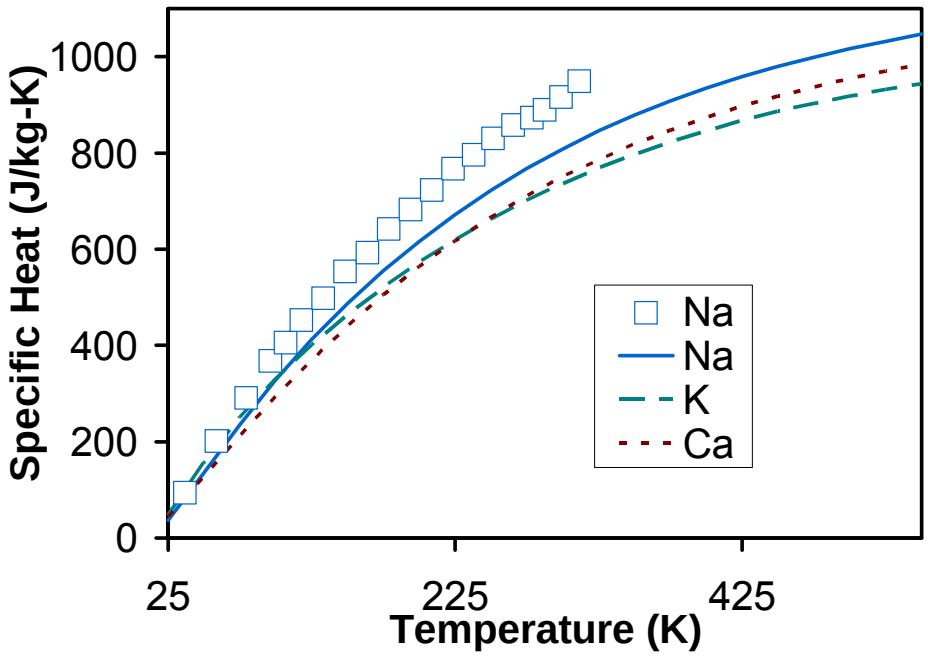

Figure 4.9 Specific heat of zeolite LTA. Experimental data is from Murashov et al[76].

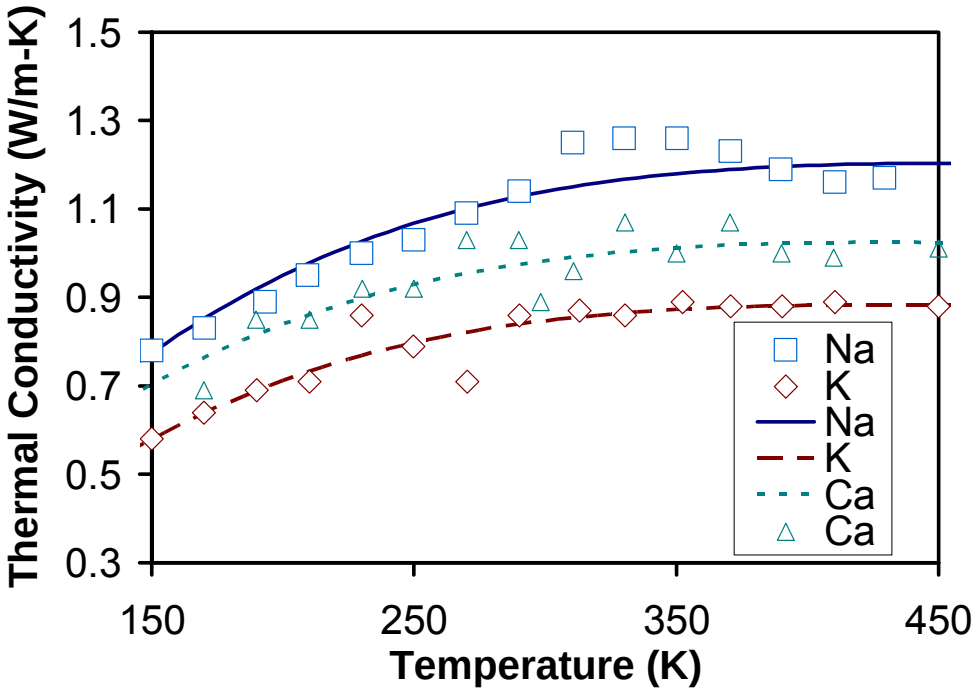

Figure 4.10 Calculated and measured thermal conductivity of zeolite LTA samples.

Except there are two notable differences, no defect scattering term is included in LTA's relaxation time expression and the relaxation time parameters are independently fitted for each type of LTA. This is done because the different types of LTA differ from each other by 96 atoms while the different types of MFI differed from each other by at most three atoms so the LTA structures cannot be thought of as perturbations of each other. The calculated specific heat is shown in Figure 4.9. Experimental data is available only for Na-LTA. The discrepancy with experiment implies that the interatomic potential used to model the cation framework interaction is not as robust as the pure zeolite interatomic potential.

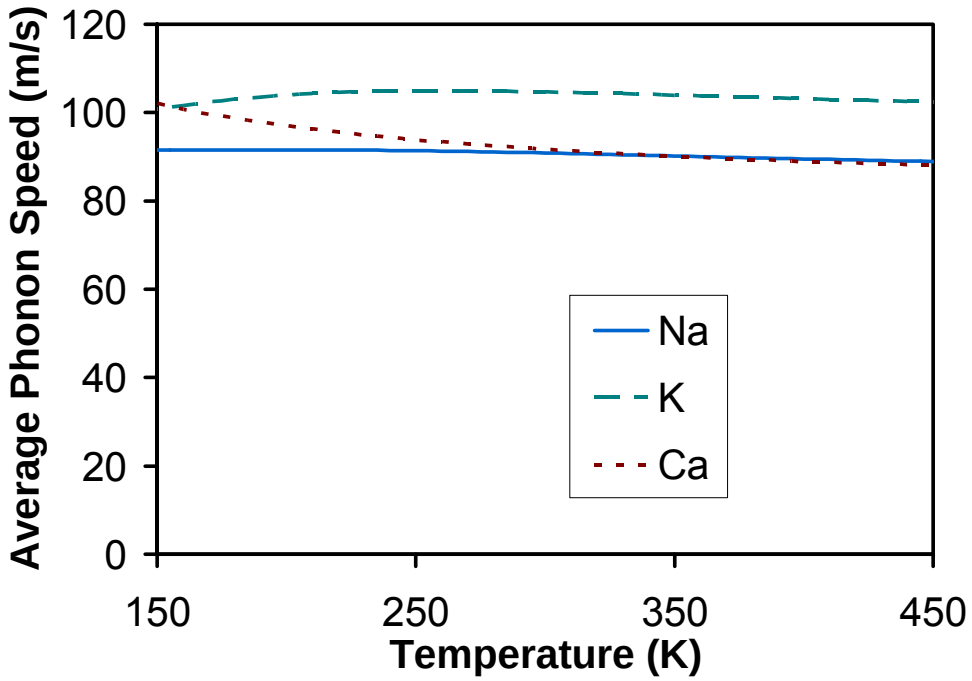

Figure 4.11 Modal specific heat weighted average phonon speed of LTA in the (1 0 0) direction.

The thermal conductivity is shown in Figure 4.10, the specific heat weighted phonon speed in Figure 4.11, and the phonon mean free path in Figure 4.12. It is of note that there is little change in average phonon velocity amongst different types of LTA and that the differences in conductivity seem to primarily a result from different boundary scattering rates. This is the opposite of what occurs amongst the different types of MFI. Zeolite LTA's fitted constants and their confidence intervals are shown in Table 4.3. The confidence intervals reflect the importance of boundary scattering. The moderately large confidence intervals for the Umklapp constants probably result from inaccuracies in the assumed functional form and the difficulty in fitting a process of secondary importance to

noisy data. LTA has larger effective boundary scattering domains than MFI. This may occur because the cations can carry heat across the channels so the boundary scattering effect is slightly less pronounced. Further evidence of this can be found in a recent molecular dynamics study[11] which discovered that frequently the inclusion of cations in zeolite pores increases phonon lifetime.

Table 4.1 Fitted phonon scattering model parameters for LTA films.

Cation		Fitted Constants	95% confidance interval
Na	B (s/K-rad^2)	2.66E-21	64
Na	l_{eff} (m)	1.16E-08	8
K	B (s/K-rad^2)	6.78E-21	64
K	l_{eff} (m)	7.45E-09	8
Ca	B (s/K-rad^2)	2.63E-21	67
Ca	l_{eff} (m)	1.07E-08	7

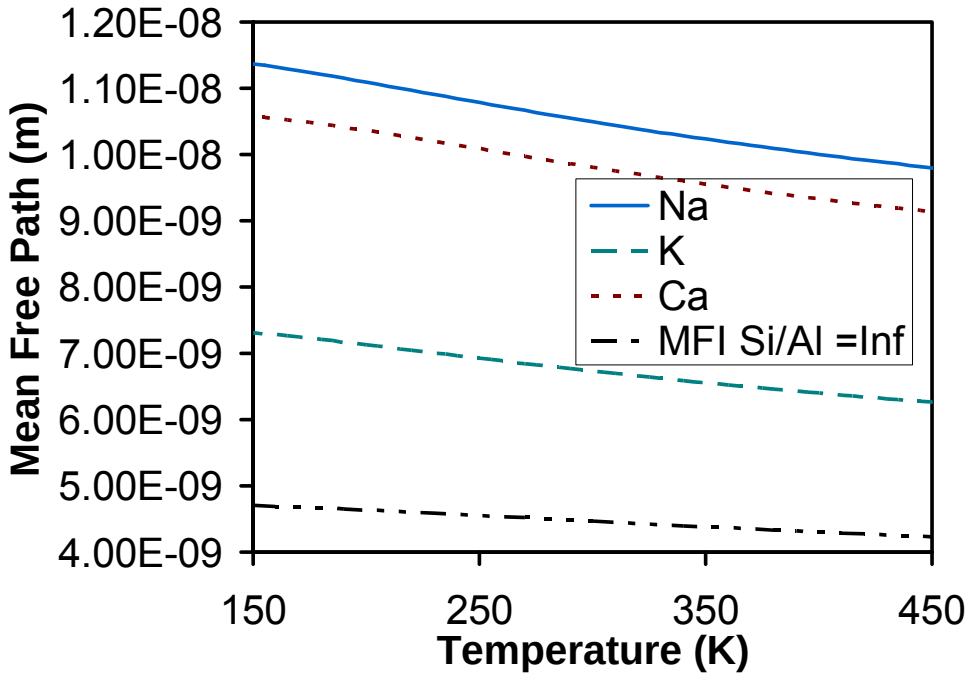

Figure 4.12 Phonon mean free path in different types of LTA.

4.10 New Brillouin Zone Integration Technique for Extremely Large Unit Cells

Zeolite unit cells can get large and if a supercell needs to be used as a unit cell to simulate disorder the new unit cell can be extremely large. This becomes a computational problem because an increase in unit cell size makes the dispersion calculation more expensive. The LTA unit cells used have up to 480 atoms. For the LTA unit cells, it took almost 10 days of computation time to calculate the dispersions on a 1000 point grid. Therefore, the practicality of calculating the dispersion of even larger cells on a 1000 point grid becomes questionable. There are many techniques[77,78] that can be used to approximate Brillouin zone integrations by appropriately sampling different wave vectors. However these techniques cannot be used to calculate quantities that are

not solely dependant on phonon frequency, and conductivity is dependant on phonon velocity. Furthermore, unless the Hellman-Feynman theorem is used, which can get expensive for large unit cells, current sampling schemes cannot be used to obtain phonon velocities at the selected wave-vectors. To circumvent this problem a new Brillouin zone integration scheme, which easily includes phonon velocity has been developed. Use of the new integration scheme will cause some error but it reduces the number of wave-vectors that the dispersion needs to be calculated at by two orders of magnitude.

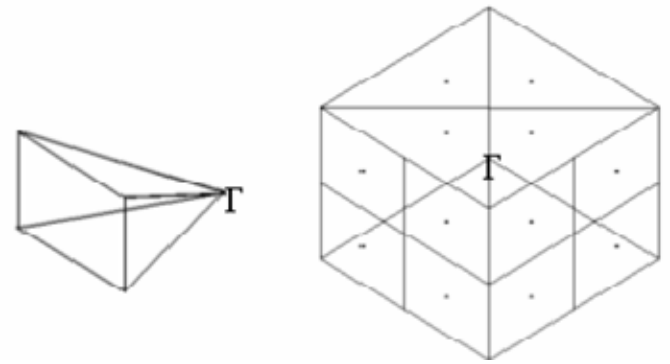

Figure 4.13 Schematic showing one of the twelve subsections, and the positive octant of the Brillouin zone of MFI. For clarity, divisions between subsections and centers of subsections are marked only on Brillouin zone surface.

The new integration scheme is used to integrate over the box-shaped Brillouin Zone of siliceous MFI to calculate the conductivity. For the sake of simplicity, the full relaxation time mode that was presented earlier is not used instead a single relaxation time is fitted to all phonon modes. The goal is not to obtain an exact comparison with the full grid but just to get an order of magnitude estimate of the relaxation time with the new

summation technique to see if it is reasonable. Due to symmetry considerations, the calculation need only be performed in the positive octant. In this scheme, the three orthogonal faces in the positive octant are discretized into 4 subsections, giving a total of 12 subsections. The volume of each subsection is bounded by lines from the edges of the subsection's face on the Brillouin zone surface to the origin. Figure 4.13 shows a schematic of the Brillouin zone discretization. Dispersion curves are calculated from the origin to the center of each subsection face. It is assumed that in a given subsection, each dispersion curve is dependent only on kx, ky, or kz, depending on whether the subsection ends on the kx, ky, or kz plane. This yields the following expression for thermal conductivity,

$$k_j = \frac{k_b}{\pi^3}\sum_{i=1}^{3}\sum_{S=1}^{4}\sum_{P=1}^{864}\iiint\left(\frac{\hbar\omega}{k_bT}\right)^2 \frac{e^{\hbar\omega/k_bT}}{\left(e^{\hbar\omega/k_bT}-1\right)^2} v_j^2\tau_j dV_{BZi} \qquad (4.6),$$

$$dV_{BZ1} = \frac{K_x^2}{\cos^3\theta\sin^2\phi}dK_x d\phi d\theta$$

$$dV_{BZ2} = \frac{K_y^2}{\sin^3\theta\sin^2\phi}dK_y d\phi d\theta \qquad (4.7)$$

$$dV_{BZ3} = \frac{K_z^2}{\cos^3\phi}\sin\phi dK_z d\phi d\theta \quad .$$

The integration is over the volume elements dV_{BZi} The i summation is over the 3 faces and the S summation is for the 4 discretized subsections that end on each face. Because the dispersion is calculated along lines in the Brillouin zone phonon velocities can be estimated. However, the velocity components not parallel with the line that the

dispersion is calculated on are neglected and this will cause some error, so the integration scheme should not be used unless the unit cell is extremely large. By fitting a constant relaxation time the new integration scheme estimated a relaxation time of 9.2 ps in siliceous MFI. The average relaxation time using the full grid is 10.9 ps. It must be noted that such close agreement is a bit fortuitous but it does show that the new integration scheme does a reasonable job of sampling the Brillouin zone. Further, the specific heat calculated with the new scheme is exactly the same as the specific heat that is calculated with the full grid. This integration scheme has also been extended for use with FCC and hexagonal crystals[6,79]. With appropriate geometric adjustments, this scheme can be used with even more reciprocal lattice geometries.

4.11 Summary

A new modeling paradigm has been developed to estimate the thermal conductivity in highly complex nanoporous crystals. The developed model, which incorporates information from detailed atomistic lattice dynamics calculations, well describes the observed behavior and strongly suggests that the main phonon scattering mechanism limiting the thermal conductivity of nanoporous crystals such as MFI is the boundary-like scattering from the pore network. It is also found that Al incorporation significantly suppresses the thermal conductivity due to a combination of phonon slowing and point defect scattering, and not due to specific heat effects. It was also found that for zeolites small changes to the microstructure can result in large changes to the thermal conductivity. This implies that thermal conductivity is highly sensitive to microstructural detail; as a result multiscale modeling of zeolites needs to be handled with caution because seemingly small approximations may result in large errors. The new modeling

paradigm was also used to analyze the effects of cation type on the conductivity of LTA. It was found that specific changes a little bit with cation type, phonon velocity barely changes, and that differences in effective boundary scattering are responsible for the corresponding change in thermal conductivity. This occurs because different cations with different configurations are able to carry different amounts of heat across the pores, but more investigation is needed to verify this hypothesis. It is important to emphasize that the present approach, although approximate in the handling of phonon scattering, still represents a considerable advance in modeling the thermal conductivity of zeolite materials. The important roles of boundary and defect scattering, as illustrated here, also imply that the thermal conductivity of these complex crystals can be tuned by exploiting not only the composition but also the pore structure, e.g., by the inclusion of molecular species in the pores.

CHAPTER 5

EVALUATION OF GALLIMUM NITRIDE INTERATOMIC POTENTIALS

The results of a molecular model are only as good as the effective interatomic potential that is used. Some materials like silicates and silicon have a variety of potentials that have been extensively tested. Unfortunately, potentials that are used to model gallium nitride have not been as rigorously tested. The three most commonly used potentials to model Gallium nitride are a Stillinger-Weber potential[29], which treats the potential energy as a sum of bond stretching and angle bending terms, a Tersoff potential[30], which is a bond order potential, and an ionic Buckingham potential[80]. For molecular simulation the Stillinger-Weber and Tersoff potentials are the most commonly used because the coulombic interactions in the ionic Buckingham potential are expensive.

All the aforementioned potentials have undergone and passed some computational tests[81-83]. The tests tend to be structural in nature, such as the ability to represent the two different solid phases of gallium nitride[30] or to correctly predict defect energies[29]. Further, all the potentials reproduce reasonable elastic constants. However, measured elastic constants in gallium nitride exhibit a large range of variability[84]. This occurs because gallium nitride is commonly grown on a substrate made of a different material. The resulting lattice mismatch strains the gallium nitride and causes large amounts of dislocations to form in the gallium nitride[85]. The significant experimental variability implies that calculated elastic constants cannot be used as a metric to pick the most accurate interatomic potential.

In this chapter lattice dynamical calculations are used to evaluate the accuracy of the Stillinger-Weber and Tersoff potentials for gallium nitride. Lattice dynamics is the most stringent test possible to evaluate the quality of interatomic potentials for material systems where only small atomic displacements occur. The test is rigorous because when only small atomic displacements occur, normal mode coordinates provide an approximation of the complete atomic dynamics of a crystalline solid. In this section phonon density of states, specific heat, average phonon velocity, homogenous Gruneisen parameter and thermal expansion are calculated with both potentials. The results are compared and contrasted with each other and when possible compared to experimental data. This analysis provides some of the most rigorous testing these potentials have undergone. It will provide an invaluable tool to better understand existing and future thermal conductivity calculations and any other gallium nitride simulation, where only small displacements occur.

5.1 Density of States

The density of states of bulk gallium nitride was calculated with both potentials. To do this the entire phonon spectra was calculated across an 8000 point grid throughout the entire Brillouin zone. The atomic spring constants were calculated numerically with 2^{nd} order finite differences by displacing the atoms by .001 angstroms at a time. The dynamical matrix was then constructed and diagonalized to obtain the normal mode frequencies. All frequencies were then sorted into a histogram with 64 boxes and normalized to obtain the density of states. The calculated results along with density functional theory calculations from the literature[86] are shown in Figure 5.1. Below the band gap both potentials produce similar density of states (small differences cannot be

taken too literally because the density of states changes and shifts a little when the Brillouin zone is sampled differently). At lower frequencies, both interatomic potentials reasonably approximate the measured density of states. Above the bang gap both potentials do a poor job. This happens because neither potential explicitly accounts for the ionicity of the crystal and when the ionic atoms vibrate they induce an electrical field, which results in the splitting and shifting of optical phonon branches. However, the phonons above the band gap have a negligible contribution to the thermal conductivity because they have small group velocities and the large band gap ensures that they will rarely interact with the phonons below the band gap.

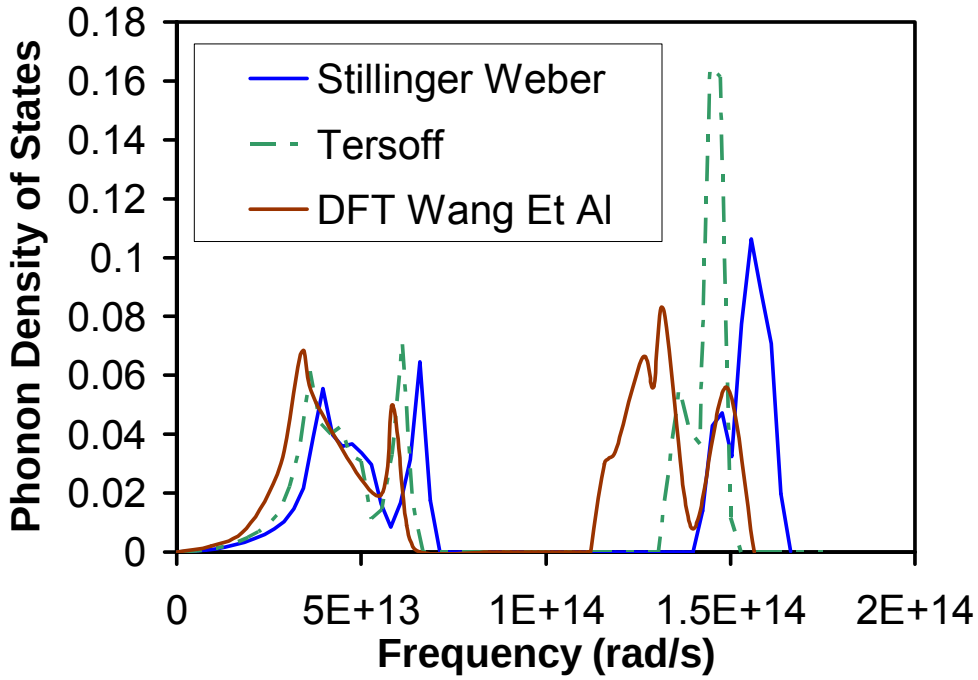

Figure 5.1 Gallium nitride density of states. Density functional theory results are from Wang et al[86].

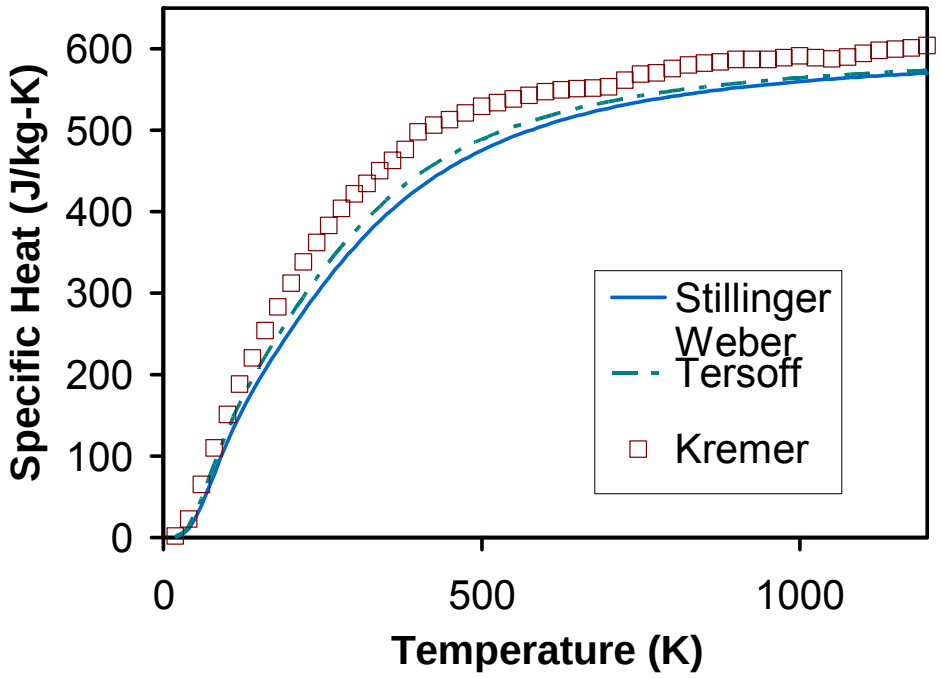

Figure 5.2 The specific heat of gallium nitride. Experimental data is from Kremer et al[87].

5.2 Specific Heat

The specific heat is an important quantity in conductivity modeling; if the specific heat is not accurate the conductivity will not be accurate. The specific heat is calculated by evaluating the specific heat of each individual phonon state and then summing over all states. Both potentials accurately reproduce the specific heat, which is shown in Figure 5.2. Deviations from experimental data could be caused by anharmonic effects (the specific heat is calculated in the harmonic approximation), differences between the measured constant pressure and the calculated constant volume specific heat, or most likely inaccuracies in the phonon spectrum from the use of effective potentials. At lower

temperatures the specific heat calculation is more accurate; this is because at low temperatures only the low frequency phonons, which have a more accurately calculated spectrum, are contributing to the specific heat and anharmonic effects are less pronounced at low temperatures.

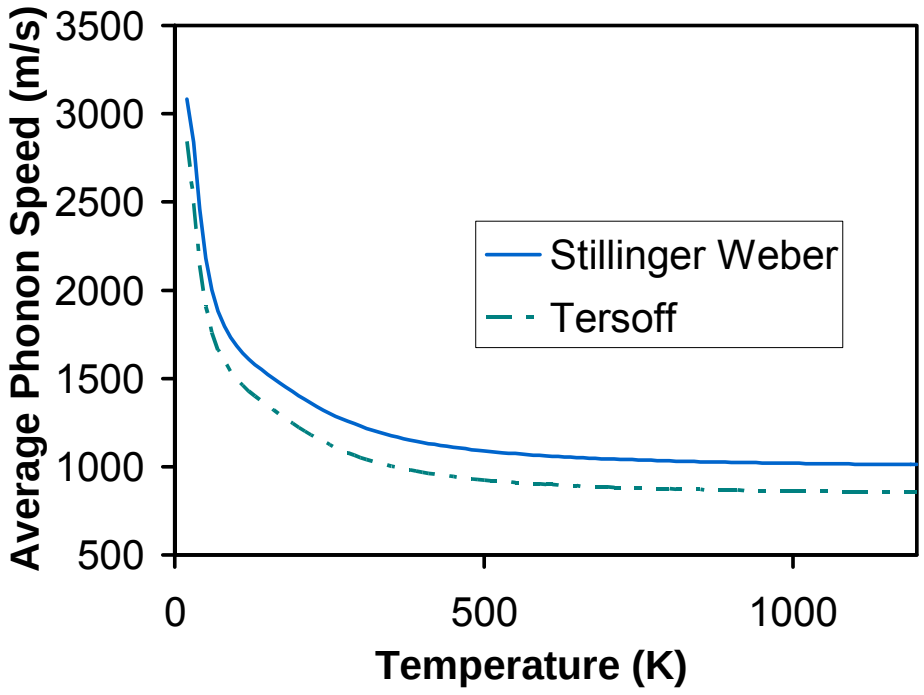

Figure 5.3 Specific heat weighted average phonon speed in the (1 0 0) direction of bulk gallium nitride.

5.3 Phonon Speed

Individual phonon velocities are calculated, using the Hellman-Feynman theorem, across the same 8000 point grid in the Brillouin zone, used to calculate the density of

states. The speeds are then obtained by projecting the velocities onto the direction of interest and taking their magnitudes. Then the average phonon speed in that direction is calculated with modal specific heat as a weighting function. Figure 5.3 shows the average phonon speed in the (1 0 0) direction; this direction was chosen because it is the axial direction in many gallium nitride nanowires so it allows for a direct comparison with phonon speeds in nanowires. Unfortunately, there are no average phonon speed experimental measurements available so phonon speed cannot be used to evaluate the potentials. The average speed in the low temperature limit is more indicative of the speed of the phonons contributing to the conductivity because in bulk gallium nitride it is expected that the long wave length acoustic phonons are the primary heat carriers. The Stillinger Weber potential predicts slightly faster phonons. This probably occurs because it predicts slightly higher elastic constants than the Tersoff potential[29,30], so the stiffer Stillinger Weber gallium nitride will have a higher speed of sound.

5.4 Gruneisen Parameter

The Gruneisen parameter is important because it gives a measure of phonon anharmonicity, which conductivity is also heavily dependent on. There is a common, heuristic, semi-empirical relaxation time model used for GaN, where modal phonon relaxation time is inversely proportional to the square of the phonon mode Gruneisen parameter [27]. While, the aforementioned semi-empirical relaxation times is approximate in nature it does show that conductivity is heavily dependant on the phonon Gruneisen parameters.

To calculate the phonon Gruneisen parameters, the spring constants are calculated in the strained and unstrained configurations, then the derivative of the dynamical matrix

with respect to strain is calculated with finite differences, and finally the Hellman-Feynman theorem is applied.

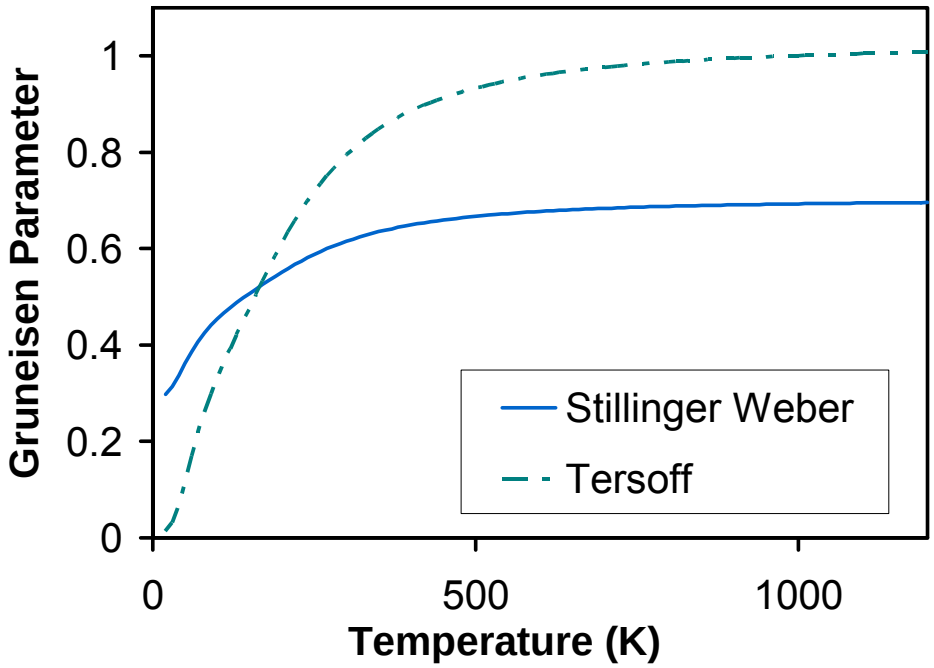

Figure 5.4 Gruneisen parameter corresponding to a homogenous strain in gallium nitride.

Figure 5.4 shows the Gruneisen parameter for a homogenous strain. It is calculated from the following phonon Gruneisen parameter expression

$$\gamma_V\left(\vec{K},p\right)=\frac{V}{\omega_p\left(\vec{K}\right)}\frac{\partial\omega_p\left(\vec{K}\right)}{\partial V} \tag{5.1}$$

The large difference in Gruneisen parameters between the two potentials, despite the small difference observed in other phonon properties, is striking. This occurs because all other phonon properties calculated earlier in this chapter are dependant on the second order derivatives of the interatomic potentials but the Gruneisen parameter, an

anharmonic property, is dependant on the third order derivatives and each time a derivative is taken of an empirical function error is magnified.

5.5 Thermal Expansion

The Gruneisen parameter cannot be directly compared to experimental data. However, the Gruneisen parameter tensor can be used to calculate the thermal expansion which in turn is readily compared with experimental data.

For an axial symmetric crystal like gallium nitride two different Gruneisen parameters are used to calculate the thermal expansion[88]. They are the specific heat weighted average of the following phonon mode Gruneisen parameters,

$$\gamma_c(\mathbf{K}, p) = -\frac{c}{\omega_p(\mathbf{K})}\frac{d\omega_p(\mathbf{K})}{dc} \tag{5.2}$$

$$\gamma_a(\vec{K}, p) = -\frac{a}{\omega_p(\mathbf{K})}\frac{d\omega_p(\mathbf{K})}{da} \tag{5.3}$$

which correspond to changes in phonon frequency with respect to strains parallel and perpendicular to the (0 0 1) direction in gallium nitride. The following expressions are used to calculate the thermal expansion of the a and c lattice constants in gallium nitride[88].

$$\alpha_a = \left\{(s_{11} + s_{12})\frac{\gamma_a}{2} + s_{13}\gamma_c\right\}c_v \tag{5.4}$$

$$\alpha_c = \left\{(s_{11} + s_{12})\gamma_a + s_{13}\gamma_c\right\}c_v \tag{5.5}$$

The s's that appear in the above equations are elements of the elastic compliance matrix, which is readily calculated from the elastic constants. The elastic constants used here are taken from Aichouine et al[29] and Nord et al[30], where are they are calculated from the

Stillinger-Weber and Tersoff potentials respectively. The calculated thermal expansions are compared with experimental data in Figures 5.5, 5.6, 5.7, and 5.8.

There is quite a bit of spread in the experimental data shown in Figures 5.5, 5.6, 5.7, and 5.8. This happens in part because all three sets of data were collected from gallium nitride samples grown in different ways. The data of Reeber et al[89] was collected from a powder sample that was synthesized by reacting molten gallium with ammonium. Roder et al's[90] data was collected from a thick film sample that was made from hydride vapor phase epitaxy and then removed from its substrate and allowed to relax. Leszczynski et al[85] made measurements on a thin film sample grown on sapphire by molecular beam epitaxy. They attribute the unusual temperature dependence of their data to strain induced from lattice mismatch effects. There is no known way of synthesizing a high quality dislocation and strain free gallium nitride sample. This highlights the difficulties in accurately characterizing gallium nitride.

It must be remembered that all the calculations presented hear are for a perfect crystal lattice. However, they can still be used to qualitatively test the robustness of the interatomic potentials. Figures 5.5, 5.6, 5.7, and 5.8. show that at all temperatures the Stillinger-Weber potential fails to even qualitatively predict the correct temperature dependence of the thermal expansion, while the Tersoff potential is able to reproduce qualitatively correct results . However, there is one major qualitative trend that the Tersoff potential fails to reproduce. It predicts that the thermal expansion of the c lattice parameter is always greater than that of the a lattice parameter. The experimental data shows that except at the lowest temperatures the expansion of the a lattice parameter is always greater than the c lattice parameter. In bulk gallium nitride only the long wave

length acoustic phonons are expected to contribute substantially to the thermal conductivity. As a result the thermal expansion at low temperatures is an indicator of how well a potential will reproduce the thermal conductivity. Figures 5.7 and 5.8 show that the Tersoff potential does a better job of reproducing experimental thermal expansion data at low temperatures than the Stillinger Weber potential as a result it is expected to yield more accurate values of the thermal conductivity than the Stillinger Weber potential. Considering the uncertainties in experimental data and the difficulties in accurately capturing anharmonic effects with an interatomic potential, the Tersoff potential does surprisingly well.

Thermal expansion is an extremely stringent test for the quality of an interatomic potential. Defect energies and structural characteristics of a material are only dependant on the potential; specific heat and phonon density of states are dependant on the 2^{nd} order derivatives of the potential; thermal expansion and conductivity are dependant on the 3^{rd} order derivatives. As a result, conductivity and thermal expansion are particular sensitive to the interatomic potential being used, and thermal expansion is one of the most rigorous tests for the accuracy of an interatomic potential that can be done without performing simulations.

5.6 Summary

Phonon density of states, specific heat, average phonon velocity, homogenous strain Gruneisen parameter, and thermal expansion were calculated with both the Tersoff and Stillinger Weber interatomic potentials for bulk gallium nitride. It was found that the calculated harmonic properties of both potentials are in reasonable agreement with experiment. Further, the harmonic properties calculated with both potentials are found to

be in qualitative agreement with each other. However, the anharmonic properties differ greatly from each other. It was found that the Tersoff potential is able to qualitatively describe thermal expansion of gallium nitride, while the Stillinger Weber potential cannot. This implies that the Tersoff potential will provide better accuracy in thermal conductivity simulations or any where anharmonic effects are critical than the Stillinger Weber potential. However, the Tersoff potential is much more complicated than the Stillinger Weber potential. As a result, it still may be preferable to use the Stillinger Weber potential in simulations that are particularly expensive.

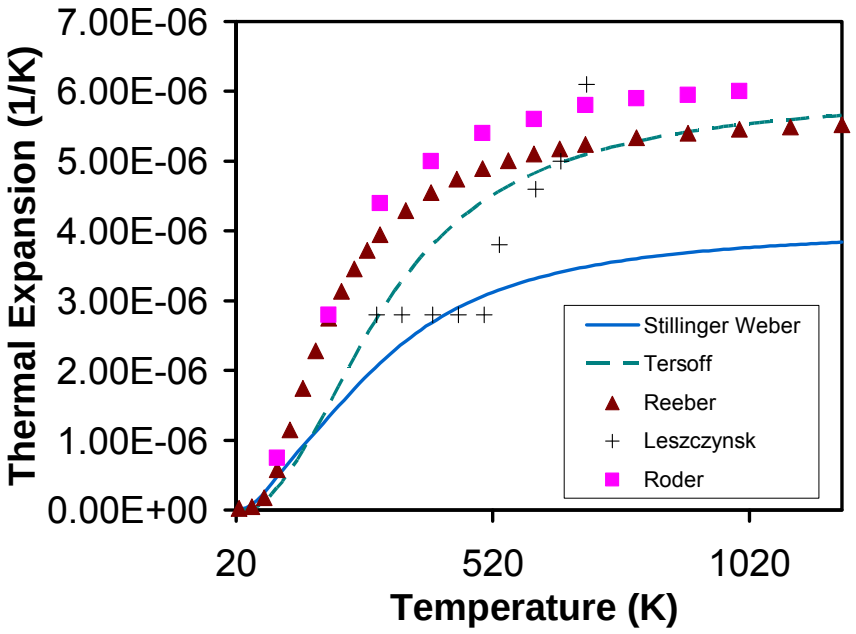

Figure 5.5 Thermal expansion of the a lattice parameter in gallium nitride.

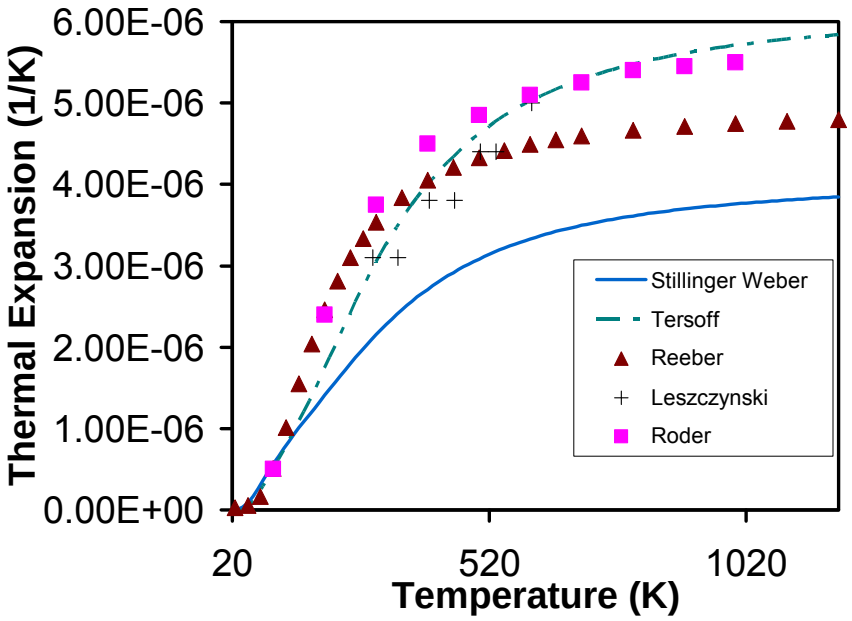

Figure 5.6 Thermal expansion of the c lattice parameter in gallium nitride.

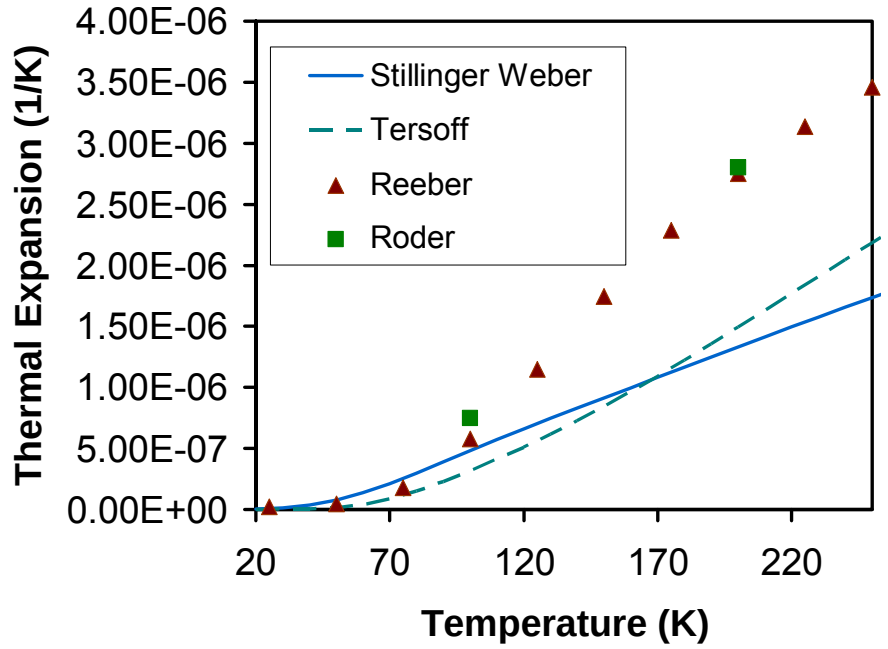

Figure 5.7 Thermal expansion of the a lattice parameter in gallium nitride at low temperatures.

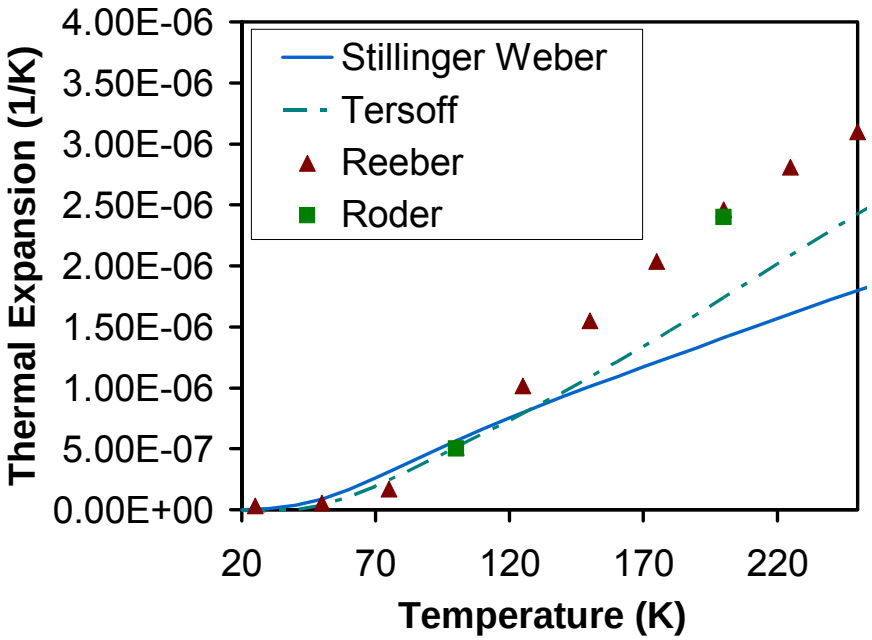

Figure 5.8 Thermal expansion of the c lattice parameter in gallium nitride at low temperatures.

CHAPTER 6

LATTICE DYNAMICS OF GALLIUM NITRIDE NANOWIRES

Nanowires are emerging as a new class of materials for use in next generation microelectronics. Their technological appeal stems from the vast differences in material properties from their bulk counterparts. Because of their wide electrical band gaps and unique optoelectronic properties gallium nitride nanowires are expected to be pervasive in next generation lasers, lighting, and high power electronics[24,26,91]. Despite their technological importance and device sensitivity to operating temperatures, their thermal properties are not well understood. There has only been one study that measured the thermal conductivity of gallium nitride nanowires[92], and large amounts of impurities in the measured wires make it difficult to distinguish between size and impurity effects on the thermal conductivity. The inherent difficulties in measuring nanowire thermal properties and the need to obtain them for a wide variety of nanowire sizes and geometries necessitate the use of computational and theoretical methods. The study presented her does not calculate nanowire thermal conductivity, but it does contribute to the understanding of phonon physics in gallium nitride nanostructures, which is necessary for understanding experimental and computational thermal conductivity data.

This chapter presents a study of the lattice dynamics of gallium nitride nanowires. Phonon dispersion, phonon density of states, specific heat, average phonon velocity, and homogenous Gruneisen parameters are calculated for different nanowire geometries and sizes.

6.1 Nanowire Structure

Calculations are performed on three different nanowire structures. All structures used are stoichiometric and have no singly coordinated atoms; otherwise they would be unstable. Two different nanowire geometries are studied the first has a cross sectional shape that is approximately an equilateral triangle and the wire axis along the (1 0 0) direction. The other structure is a hexagon with the wire axis along the (0 0 1) direction. The two structures are chosen because they both correspond to realistic nanowires that have been experimentally grown[25,93]. Wire 1 (Figure 6.1) is the equilateral triangle structure with a height of 2.9nm, wire 2 (Figure 6.2) is the same structure with a height of 6.2nm, and wire 3 (Figure 6.3) is the hexagonal structure with a diameter of 3.5 nm. The phonon properties of all three wires are calculated with the Stillinger-Weber potential.

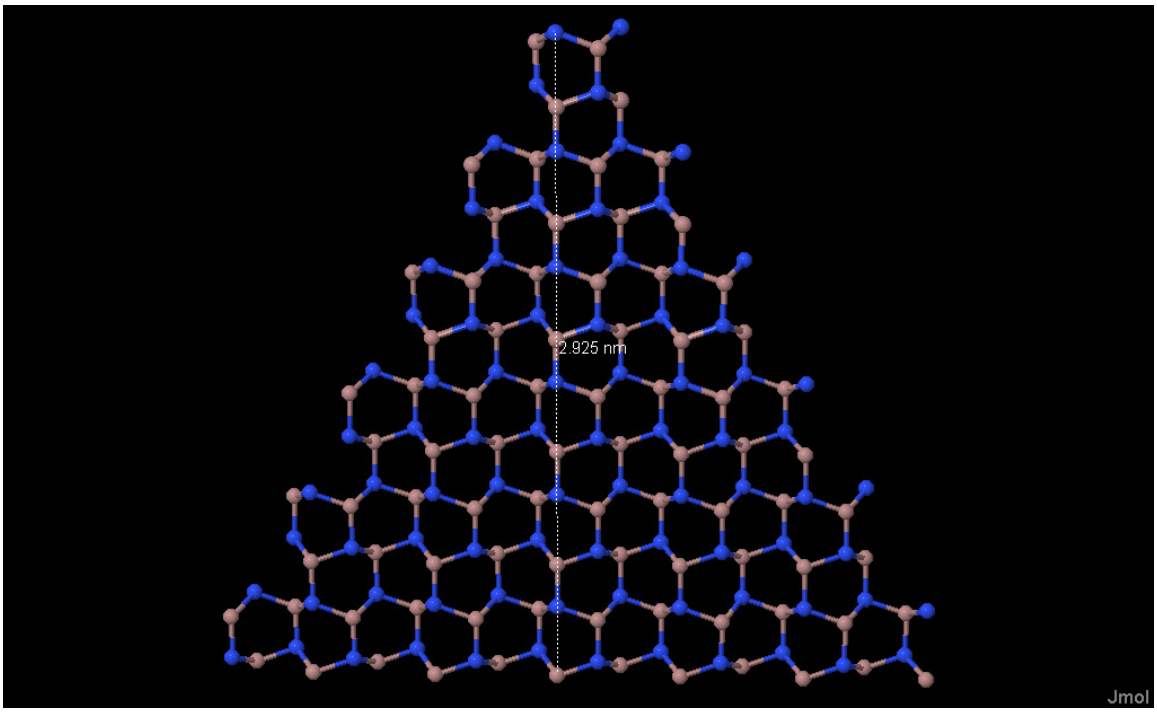

Figure 6.1 Cross section of the unit cell used in gallium nitride wire 1.

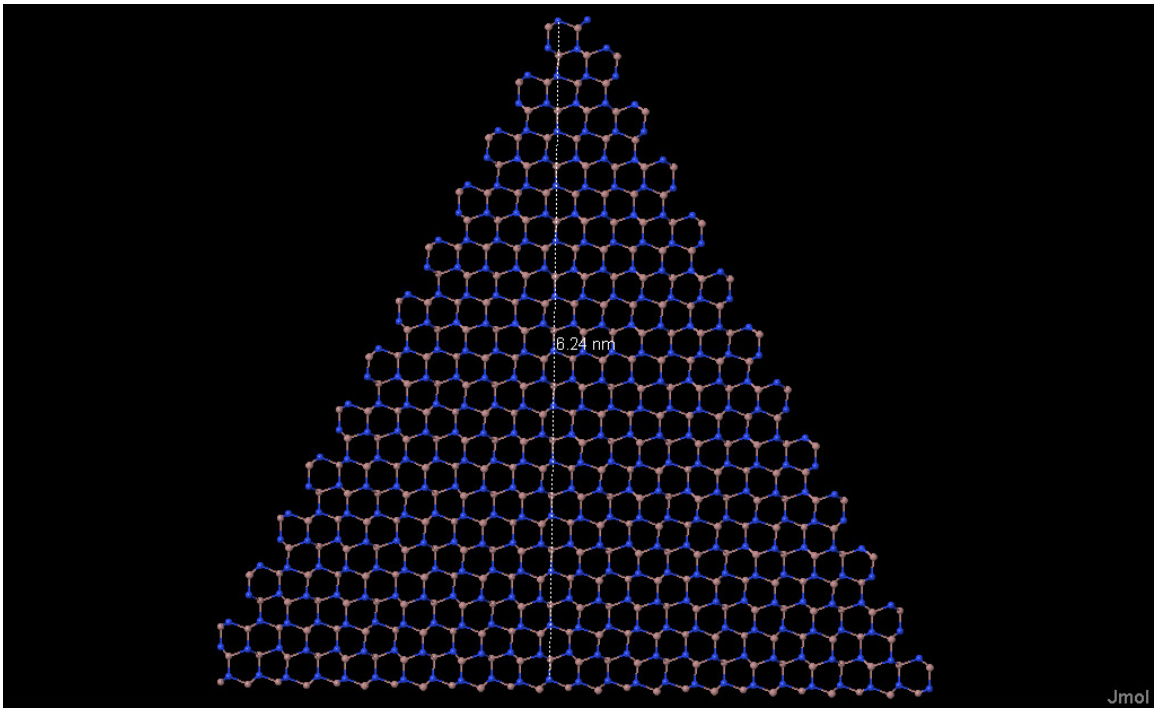

Figure 6.2 Cross section of the unit cell used in gallium nitride wire 2.

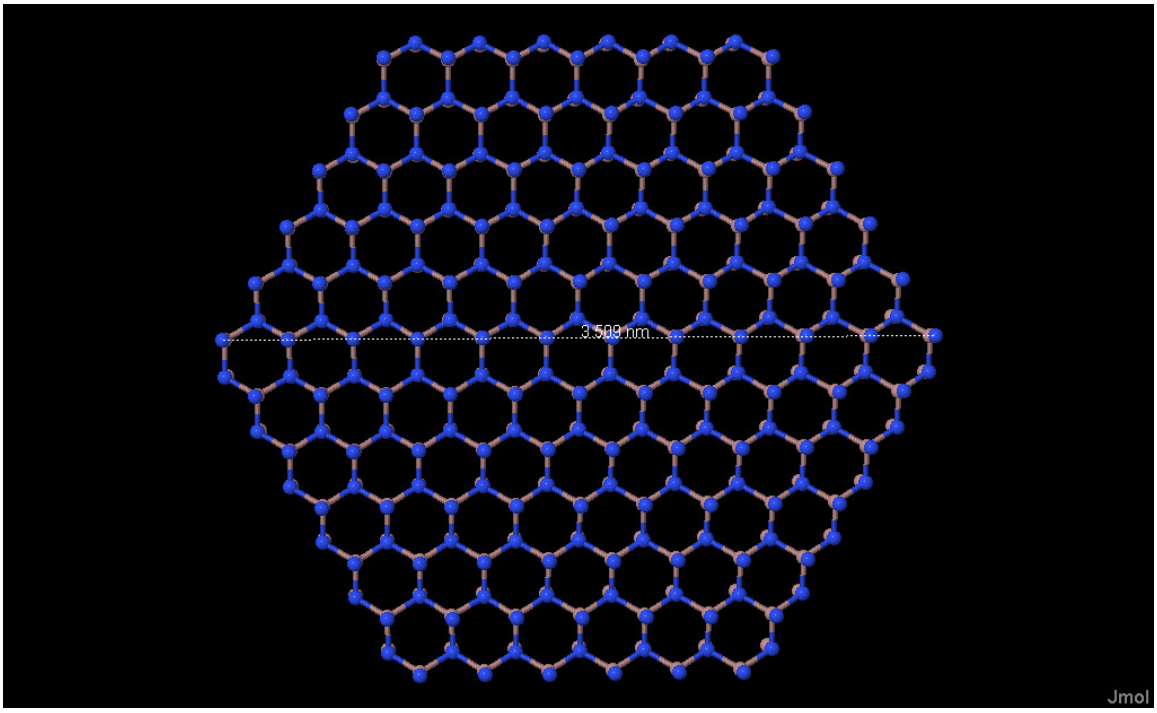

Figure 6.3 Cross section of the unit cell used in gallium nitride wire 3.

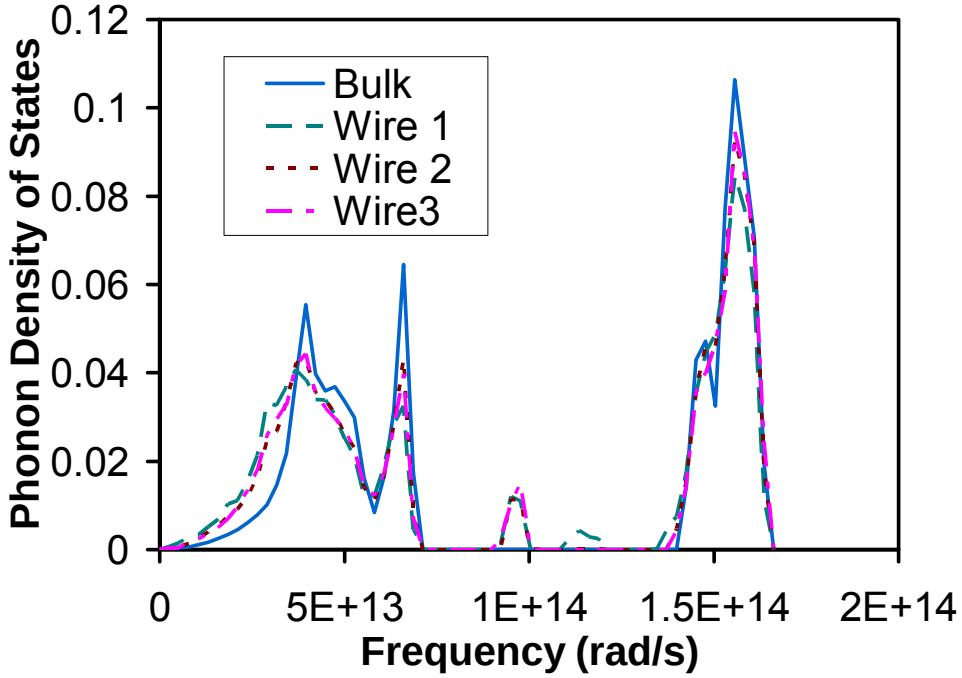

Figure 6.4 Phonon density of states of gallium nitride nanowires.

6.2 Density of States and Specific Heat

For each nanowire phonon dispersion is calculated, using the same techniques and codes that were used for the bulk calculations (see chapter 5). The calculations are done on a 20 point evenly spaced grid in the 1D Brillouin zone. The calculated dispersion for each wire is made into a histogram over different frequencies to obtain the density of states, which is shown in Figure 6.4. Despite the large differences in size and shape between the different nanowires, they all have similar density of states. However, there are moderate differences between the bulk and nanowire density of states. At low frequencies the density of states of the nanowires is shifted, which shows that the nanowires have more phonons at the lowest frequencies. The nanowires also have some

phonon states in the middle of the phonon band gap, which does not occur in bulk gallium nitride. However, this may not be a real feature of the spectrum; it may result from inaccuracies in optical phonon frequencies, which inevitably result by using an effective potential that does not explicitly account for gallium nitride's ionicity.

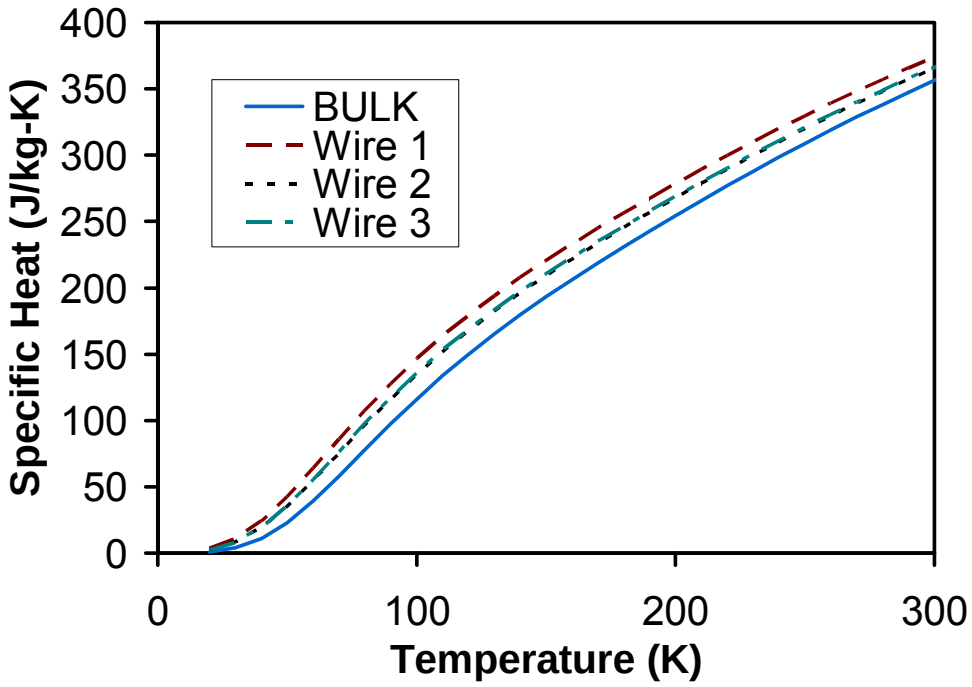

Figure 6.5 Specific heat of bulk and nanowire gallium nitride.

The calculated specific heat is shown in Figure 6.5. At higher temperatures the specific heats of the wires are very similar to each other and that of the bulk. However, at low temperatures there are significant differences between wire and bulk specific heat. At first, this may seem to imply that phonon specific heat may be responsible for the changes between nanowire and bulk conductivity but this is not the case. Nanowires are

known to have much lower conductivities than their bulk counterparts[92,94], at lower temperatures nanowire specific heat can be significantly higher than bulk, so other effects which lower the conductivity, such as phonon slowing and increased anharmonicity, must be more prominent in nanowires than increased specific heat.

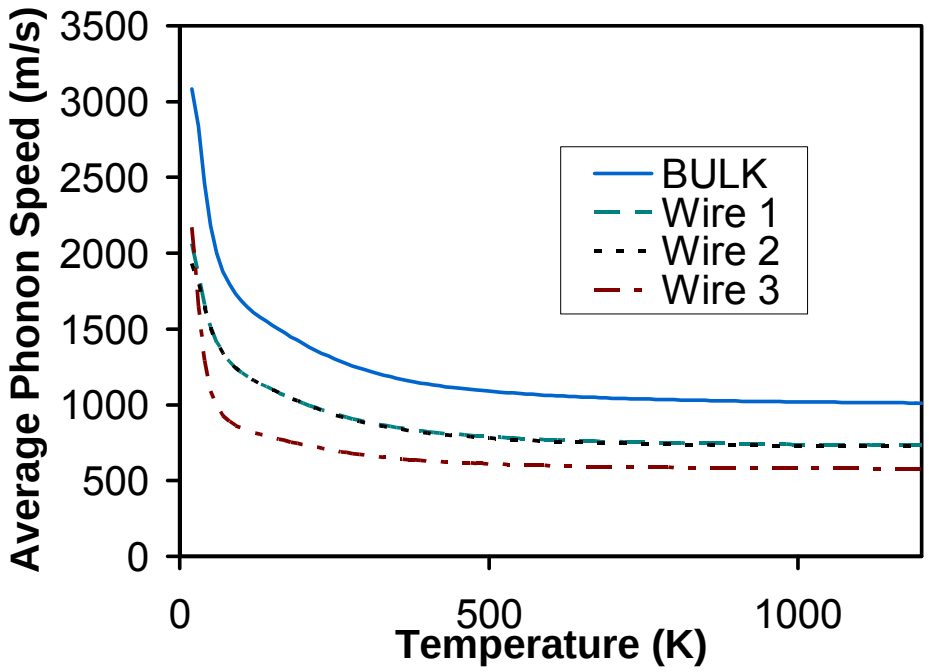

Figure 6.6 Specific heat weighted average phonon speeds in gallium nitride nanowires. The bulk speed is in the (1 0 0) direction.

6.3 Phonon Speed

The phonon velocities are calculated using the Hellman-Feynman theorem and are shown in Figure 6.6. The use of the Hellman-Feynman theorem is of particular importance because phonon band folding will cause a significant amount of phonon dispersion crossings. The wires show a significant decrease in phonon speed when

compared to the bulk. Further phonon speeds in wire 3 are decreasing even more than what is evident on the graph because the phonon speeds in bulk are for the (1 0 0) direction, while the axis of wire 3 is along the (0 0 1) direction and in bulk gallium nitride the phonons move faster in the (0 0 1) direction than they do in the (1 0 0) direction. It is surprising that wires 1 and 2 have almost the same exact average phonon speeds even though the cross sectional area of wire 2 is five times that of wire 1. Further, both wires have similar density of states and specific heats. This implies that as the wire cross sectional area increases in size convergence to bulk harmonic phonon properties is slow.

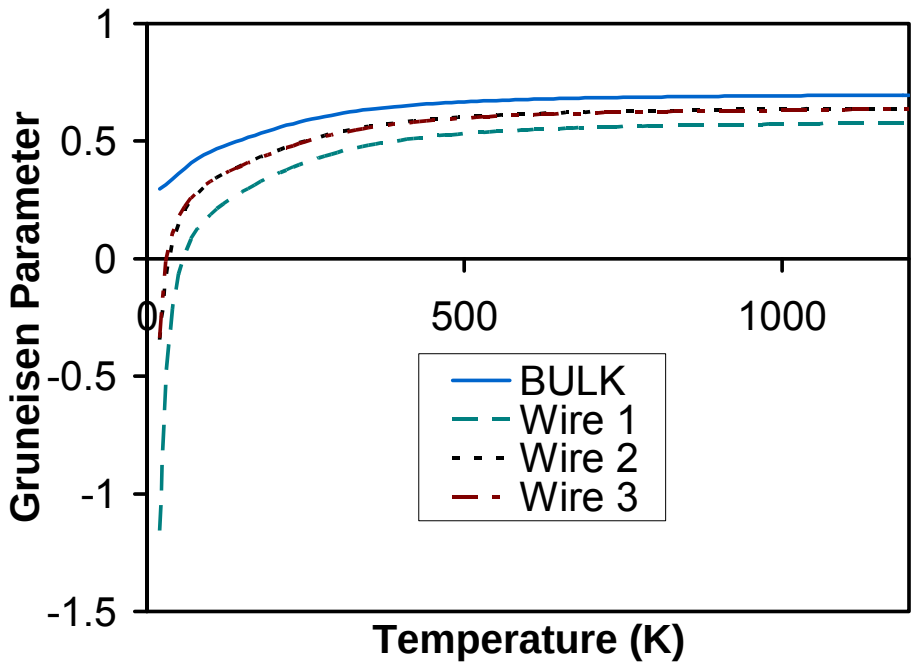

Figure 6.7 Homogenous Gruneisen parameter of gallium nitride nanowires.

6.4 Gruneisen Parameter

To see if wire anharmonicity changes significantly with nanowire shape and size the homogenous Gruneisen parameter is calculated for all the wires. They can bee seen

in Figure 6.7. The Gruneisen parameters are very similar for wires 3 and 2 but significantly different from wire 1. This contrasts heavily with the phonon speed calculation which found that wires 1 and 2 have nearly identical average phonon speeds with each other but not with wire 3. However, care needs to be taken when interpreting the Gruneisen parameter results because a more subtle size effect is occurring.

For all wires the calculated phonon Gruneisen parameters of some acoustic phonon modes close to the gamma point become highly negative; this phenomenon has also been predicted for carbon nanostructures by Schelling and Keblinski[95]. The highly negative phonon Gruneisen parameters imply thermal expansion along the wires axis will be negative. This occurs because low frequency phonons cause large atomic displacements and if the displacements are perpendicular to the wire axis the overall length will contract. This effect is expected to be more pronounced for thinner wires. By treating a carbon nanotube as a slender hollow rod, Schelling and Keblinski[95] were able to show that the magnitude of thermal contraction along the tube axis is inversely proportional to the moment of inertia of the nanotube. Because of the large difference in size between wires 1 and 2 they have very different moments of inertia and as a result deflections in wire 2 will be smaller than those in wire 1. This explains why wires 1 and 2 have different Gruneisen parameters despite their similar harmonic phonon properties.

Unfortunately, the homogenous Gruneisen parameters do not give much information about wire thermal conductivities. However, they do reveal that wire anharmonicity is strongly dependant on nanowire size. This finding may seem obvious but in light of the unexpected weak dependence of phonon speed and spectrum on wire size, it is not.

6.5 Summary

The phonon densities of states, specific heat, average phonon velocity, and homogenous Gruneisen parameter have been calculated for three different nanowires. The properties of the different wires were compared with each other and with bulk gallium nitride. It was found that while phonon density of states and specific heat of the nanowires differed substantially from that of bulk they were only weakly dependent on wire shape and size. Significant phonon slowing was found to occur in the nanowires and the average phonon speed was found to be dependant on the wire shape but not size. It is unusual that for triangular shaped wires a five-fold increase in wire cross sectional area barely changes the average phonon speed. It was found that the Gruneisen parameter is heavily affected by the size of the nanowire cross sectional area and that the strong dependence occurs in part by a few phonons with large negative phonon Gruneisen parameters. This in turn makes it difficult to ascertain the effect of wire size and geometry on the anharmonicity of other phonon modes.

CHAPTER 7

CONCLUSION

All the work presented here addressed challenges that need to be overcome to extend current thermal conductivity calculations to exotic and/or ill characterized materials. A new thermal conductivity modeling methodology has been developed to calculate the thermal conductivity of zeolites and other highly complex materials. It was used to discover the unusually prominent role of phonon slowing in the thermal conductivity reduction that results from substitutional defects in zeolites. It also corroborated recent molecular simulations[11] that showed inclusion of impurities in zeolite pores can facilitate heat transfer.

Two interatomic potentials (Stillinger-Weber and Tersoff) commonly used to simulate gallium nitride were extensively tested. It was found that good theoretical agreement with experimental data of harmonic properties does not imply that anharmonic properties are accurately treated by the potential used. In particular the Stillinger-Weber potential is able to accurately reproduce the density of states and specific heat of bulk gallium nitride but does a poor job of calculating the thermal expansion coefficients. This implies that thermal conductivity calculations that use the Stillinger-Weber potential may be particularly error prone. The phonon properties of gallium nitride nanowires were calculated and compared with one another it was found that harmonic phonon properties are only weakly dependant on wire diameter, but differ substantially from bulk.

There is still a lot of work that can be done to expand and improve upon the work presented here. A more sophisticated relaxation time expression is needed to more accurately model and better understand the thermal conductivity of highly complex crystals. Other interatomic potentials used to model gallium nitride need to be tested. Existing interatomic potentials could possibly have their parameters tweaked by fitting them to an anharmonic observable. Understanding of the thermal properties of gallium nitride nanowire would greatly be enhanced by molecular simulation of their thermal conductivities and by calculation of their thermal expansion coefficients.

As technology and material synthesis techniques progress, the prominence of complex and exotic materials will continue to increase. Many applications in which they are used in are sensitive to their thermal properties. As a result, understanding of thermal transport in complex materials will continue to be an important scientific challenge. Furthermore, to achieve the long term goal of having designer materials with tailored properties understanding of thermal transport in complex materials is essential.

BIBLIOGRAPHY

[1] M. E. Davis, Nature **417,** 813-821 (2002).

[2] M. Tsapatsis, Aiche Journal **48,** 654-660 (2002).

[3] X. L. Wang, H. T. Chua, and K. C. Ng, International Journal of Refrigeration-Revue Internationale Du Froid **28,** 756-765 (2005).

[4] J. M. Gordon, K. C. Ng, H. T. Chua, and A. Chakraborty, International Journal of Refrigeration-Revue Internationale Du Froid **25,** 1025-1033 (2002).

[5] K. Mukhopadhyay, A. Koshio, N. Tanaka, and H. Shinohara, Japanese Journal of Applied Physics Part 2-Letters **37,** L1257-L1259 (1998).

[6] A. M. Greenstein, S. Graham, Y. C. Hudiono, and S. Nair, Nanoscale and Microscale Thermophysical Engineering **10,** 321-331 (2006).

[7] A. J. H. McGaughey and M. Kaviany, International Journal of Heat and Mass Transfer **47,** 1799-1816 (2004).

[8] V. V. Murashov, Journal of Physics-Condensed Matter **11,** 1261-1271 (1999).

[9] V. V. Murashov and M. A. White, Materials Chemistry and Physics **75,** 178-180 (2002).

[10] A. Griesinger, K. Spindler, and E. Hahne, International Journal of Heat and Mass Transfer **42,** 4363-4374 (1999).

[11] C. Y. Chen and D. I. Kopelevich, Molecular Simulation **34,** 155-167 (2008).

[12] Y. Hudiono, A. Greenstein, C. Kuete, B. Olson, S. Graham, and S. Nair, Journal of Applied Physics **102,** 053523 (2007).

[13] R. Peierls, Annalen Der Physik **3,** 1055-1101 (1929).

[14] P. G. Klemens, Proceedings of the Royal Society of London Series a-Mathematical and Physical Sciences **208,** 108-133 (1951).

[15] P. G. Klemens, Solid State Physics-Advances in Research and Applications **7,** 1-98 (1958).

[16] J. Callaway, Physical Review **122,** 787-& (1961).

[17] M. G. Holland, Physical Review **132,** 2461-& (1963).

[18] M. D. Tiwari and B. K. Agrawal, Physical Review B **4,** 3527-& (1971).

[19] M. AsenPalmer, K. Bartkowski, E. Gmelin, M. Cardona, A. P. Zhernov, A. V. Inyushkin, A. Taldenkov, V. I. Ozhogin, K. M. Itoh, and E. E. Haller, Physical Review B **56,** 9431-9447 (1997).

[20] M. Roufosse and P. G. Klemens, Physical Review B **7,** 5379-5386 (1973).

[21] G. A. Slack and S. Galginaitis, Physical Review a-General Physics **133,** A253-& (1964).

[22] G. P. Srivastava, *The Physics of Phonons* (Adam Hilger, Bristol, UK, 1990).

[23] J. L. Hudgins, G. S. Simin, E. Santi, and M. A. Khan, Ieee Transactions on Power Electronics **18,** 907-914 (2003).

[24] J. C. Johnson, H. J. Choi, K. P. Knutsen, R. D. Schaller, P. D. Yang, and R. J. Saykally, Nature Materials **1,** 106-110 (2002).

[25] F. Qian, S. Gradecak, Y. Li, C. Y. Wen, and C. M. Lieber, Nano Letters **5,** 2287-2291 (2005).

[26] Y. Huang, X. F. Duan, Y. Cui, and C. M. Lieber, Nano Letters **2,** 101-104 (2002).

[27] D. T. Morelli, J. P. Heremans, and G. A. Slack, Physical Review B **66,** - (2002).

[28] J. Zou, D. Kotchetkov, A. A. Balandin, D. I. Florescu, and F. H. Pollak, Journal of Applied Physics **92,** 2534-2539 (2002).

[29] N. Aichoune, V. Potin, P. Ruterana, A. Hairie, G. Nouet, and E. Paumier, Computational Materials Science **17,** 380-383 (2000).

[30] J. Nord, K. Albe, P. Erhart, and K. Nordlund, Journal of Physics-Condensed Matter **15,** 5649-5662 (2003).

[31] D. C. Wallace, *Thermodynamics of Crystals* (Dover, New York, 1972).

[32] S. Huxtable, Thesis, University of California, 2002.

[33] P. Debye, Annalen Der Physik **39,** 789-839 (1912).

[34] C. Kittel, *Introduction to Solid State Physics*, 7 ed. (John Wiley and Sons Inc., New York, NY, 1996).

[35] J. M. Ziman, *Electrons and Phonons* (Claredon Press, Oxford, 1960).

[36] A. A. Maradudin, A. E. Fein, and G. H. Vineyard, Physica Status Solidi **2,** 1479-1492 (1962).

[37] A. A. Maradudin and A. E. Fein, Physical Review **1,** 2589-& (1962).

[38] V. V. Goldman, G. K. Horton, and M. L. Klein, Physical Review Letters **24,** 1424-& (1970).

[39] V. V. Goldman, G. K. Horton, T. H. Keil, and M. L. Klein, Journal of Physics Part C Solid State Physics **3,** L33-& (1970).

[40] P. Carruthers, Reviews of Modern Physics **33,** 92-138 (1961).

[41] P. G. Klemens, Journal of Physics and Chemistry of Solids **8,** 345-347 (1959).

[42] P. Carruthers, Physical Review **1,** 995-1001 (1959).

[43] S. Simons, Journal of Physics C-Solid State Physics **8,** 1147-1158 (1975).

[44] G. P. Srivastava, Pramana **6,** 1-18 (1976).

[45] A. J. H. McGaughey and M. Kaviany, Physical Review B **69,** - (2004).

[46] D. Greenwood, *Classical Dynamics* (Dover Publications, 1997).

[47] M. Born and K. Huang, *Dynamical Theory of Crystal Lattices* (Oxford University Press, New York, 1954).

[48] M. T. Dove, *Introduction to Lattice Dynamics* (Cambridge University Press, New York, 1993).

[49] J. D. Chung, A. J. H. McGaughey, and M. Kaviany, Journal of Heat Transfer-Transactions of the Asme **126,** 376-380 (2004).

[50] Y. Hudiono, Thesis, Georgia Institute of Technology, 2008.

[51] P. K. Schelling, (Livermore, Ca, 2007).

[52] F. H. Stillinger and T. A. Weber, Physical Review B **31,** 5262-5271 (1985).

[53] C. R. A. Catlow, C. M. Freeman, M. S. Islam, R. A. Jackson, M. Leslie, and S. M. Tomlinson, Philosophical Magazine a-Physics of Condensed Matter Structure Defects and Mechanical Properties **58,** 123-141 (1988).

[54] G. V. Lewis and C. R. A. Catlow, Journal of Physics C-Solid State Physics **18,** 1149-1161 (1985).

[55] J. Tersoff, Physical Review B **37,** 6991-7000 (1988).

[56] J. Tersoff, Physical Review B **39,** 5566-5568 (1989).

[57] D. Wolf, P. Keblinski, S. R. Phillpot, and J. Eggebrecht, Journal of Chemical Physics **110,** 8254-8282 (1999).

[58] A. J. Vega, Journal of Physical Chemistry **100,** 833-836 (1996).

[59] J. Choi, S. Ghosh, Z. P. Lai, and M. Tsapatsis, Angewandte Chemie-International Edition **45,** 1154-1158 (2006).

[60] Z. P. Lai, M. Tsapatsis, and J. R. Nicolich, Advanced Functional Materials **14,** 716-729 (2004).

[61] G. Xomeritakis, A. Gouzinis, S. Nair, T. Okubo, M. Y. He, R. M. Overney, and M. Tsapatsis, Chemical Engineering Science **54,** 3521-3531 (1999).

[62] B. W. Olson, S. Graham, and K. Chen, Review of Scientific Instruments **76,** - (2005).

[63] D. G. Cahill, Review of Scientific Instruments **61,** 802-808 (1990).

[64] C. Kittel and H. Kroemer, *Thermal Physics*, 2 ed. (W.H. Freeman Company, New York, NY, 1980).

[65] B. L. Huang, A. J. H. McGaughey, and M. Kaviany, International Journal of Heat and Mass Transfer **50,** 393-404 (2007).

[66] B. L. Huang, Z. Ni, A. Millward, A. J. H. McGaughey, C. Uher, M. Kaviany, and O. Yaghi, International Journal of Heat and Mass Transfer **50,** 405-411 (2007).

[67] J. D. Gale, Journal of the Chemical Society-Faraday Transactions **93,** 629-637 (1997).

[68] J. L. Warren, Reviews of Modern Physics **40,** 38-& (1968).

[69] A. J. C. Ladd, B. Moran, and W. G. Hoover, Physical Review B **34,** 5058-5064 (1986).

[70] T. M. Davis, T. O. Drews, H. Ramanan, C. He, J. S. Dong, H. Schnablegger, M. A. Katsoulakis, E. Kokkoli, A. V. McCormick, R. L. Penn, and M. Tsapatsis, Nature Materials **5,** 400-408 (2006).

[71] G. Gonzalez, W. Stracke, Z. Lopez, U. Keller, A. Ricker, and R. Reichelt, Microscopy and Microanalysis **10,** 224-235 (2004).

[72] T. Damker, H. Bottger, and V. V. Bryksin, Physical Review B **59,** 8626-8638 (1999).

[73] J. J. Pluth and J. V. Smith, Journal of the American Chemical Society **102,** 4704-4708 (1980).

[74] J. J. Pluth and J. V. Smith, Journal of Physical Chemistry **83,** 741-749 (1979).

[75] J. J. Pluth and J. V. Smith, Journal of the American Chemical Society **105,** 1192-1195 (1983).

[76] L. Y. Qiu, V. Murashov, and M. A. White, Solid State Sciences **2,** 841-846 (2000).

[77] D. J. Chadi and M. L. Cohen, Physical Review B **8,** 5747-5753 (1973).

[78] H. J. Monkhorst and J. D. Pack, Physical Review B **13,** 5188-5192 (1976).

[79] A. M. Greenstein, S. Graham, Y. C. Hudiono, and S. Nair, in *ASME IMECE* (ASME, Chicago, IL, 2006), p. November 7, 2006.

[80] P. Zapol, R. Pandey, and J. D. Gale, Journal of Physics-Condensed Matter **9,** 9517-9525 (1997).

[81] A. Bere and A. Serra, Physical Review B **65,** - (2002).

[82] A. Bere and A. Serra, Philosophical Magazine **86,** 2159-2192 (2006).

[83] X. W. Zhou, D. A. Murdick, B. Gillespie, and H. N. G. Wadley, Physical Review B **73** (2006).

[84] A. Polian, M. Grimsditch, and I. Grzegory, Journal of Applied Physics **79,** 3343-3344 (1996).

[85] M. Leszczynski, T. Suski, H. Teisseyre, P. Perlin, I. Grzegory, J. Jun, S. Porowski, and T. D. Moustakas, Journal of Applied Physics **76,** 4909-4911 (1994).

[86] H. Y. Wang, H. Xu, T. T. Huang, and C. S. Deng, European Physical Journal B **62,** 39-43 (2008).

[87] R. K. Kremer, M. Cardona, E. Schmitt, J. Blumm, S. K. Estreicher, M. Sanati, M. Bockowski, I. Grzegory, T. Suski, and A. Jezowski, Physical Review B **72** (2005).

[88] T. H. K. Barron, J. G. Collins, and G. K. White, Advances in Physics **29,** 609-730 (1980).

[89] R. R. Reeber and K. Wang, Journal of Materials Research **15,** 40-44 (2000).

[90] C. Roder, S. Einfeldt, S. Figge, and D. Hommel, Physical Review B **72** (2005).

[91] T. Kuykendall, P. J. Pauzauskie, Y. F. Zhang, J. Goldberger, D. Sirbuly, J. Denlinger, and P. D. Yang, Nature Materials **3,** 524-528 (2004).

[92] C. Guthy, C. Y. Nam, and J. E. Fischer, Journal of Applied Physics **103** (2008).

[93] B. S. Xu, L. Y. Zhai, J. Liang, S. F. Ma, H. S. Jia, and X. G. Liu, Journal of Crystal Growth **291,** 34-39 (2006).

[94] N. Mingo, L. Yang, D. Li, and A. Majumdar, Nano Letters **3,** 1713-1716 (2003).

[95] P. K. Schelling and R. Keblinski, Physical Review B **68** (2003).